공학석사 학위논문

An Investigation of Tidal Currents around the West Coast of Korea Responding to Bottom Roughness and Open Boundary Conditions

조도계수 및 개방경계조건에 따른 한국 서해안의 조류 연구

2019 년 8 월

서울대학교 대학원
건설환경공학부
이 민 재

Abstract

The tide around the West Coast of Korea is large and the tidal current is strong and sensitive to tidal elevation. Moreover, since the tidal flow is the main forcing of water circulation around the West Coast of Korea, it is necessary to predict the tidal elevation accurately and find out characteristics of the tide around the West Coast of Korea.

In this study, a number of the numerical simulations were carried out to investigate the effect of bottom roughness and open boundary conditions on the tidal elevation around the West Coast of Korea. The well-known open-source model, Telemac-2D, was applied as a simulation tool and three well-known ocean tide models, FES2014, NAO99Jb and TPXO9.1, were used to set the open boundary conditions for the numerical simulations in order to reproduce the tide. Besides, the complicated geometry around the West Coast of Korea influences to tide, so unstructured grid was used to represent the geometry and reflect its effect. The numerical results were calibrated and validated against observation data. It showed a good agreement between simulation results and observation data.

Tidal elevation around the West Coast of Korea was evaluated corresponding to bottom friction coefficients, which were set as uniform and local distributions. The numerical results were enhanced when the bottom friction coefficients were applied differently depending on the regions based on the natural bathymetry and coastlines. Sensitivity analyses of tides corresponding

to the open boundary conditions were carried out in order to understand the characteristic of the tide around the West Coast of Korea.

Keywords: Tidal Model, Yellow Sea, TELEMAC, Numerical Modeling, Tide, Unstructured Grid, Bottom Friction Coefficient

Student ID: 2017-21137

Table of Contents

FIGURE

TABLE

NOMENCLATURE

Latin alphabet

F_x	Source term along with x in the momentum equation
F_y	Source term along with y in the momentum equation
$\vec{F}^c$	Coriolis force
g	Acceleration of gravity
h	Water depth
k	Turbulent energy
p	Pressure
t	time
u	Velocity component in x-dir
v	Velocity component in y-dir
Z_s	Free surface elevation
Z_f	Bottom elevation

Greek alphabet

ε	Turbulent dissipation
λ	Latitude
ν	Coefficient of molecular diffusion
ν_t	Coefficient of turbulent diffusion
ν_e	Diffusion coefficient including dispersion and turbulence
ρ	Density of water
ω	Angular velocity of the Earth

CHAPTER 1. INTRODUCTION

1.1 Introduction

The Yellow Sea is surrounded by Korea, China, and the East China Sea. Water circulation in the Yellow Sea mostly influenced by flow from the East China Sea. The East China Sea covers the area originating around the Taiwan Strait and extending northeastward to the Kyushu Island, Japan, and the Korea Strait, and bounded by the Ryukyu Island Chains on the southeastern open ocean (Figure 1).

The Yellow Sea is one of the regions which have a large variation of the tide. The tidal elevation is amplified up to 8 m, and velocity of the tidal currents increases up to 1.56 m/s when the tidal flow is approaching the West Coast of Korea. This tidal flow is complicated and sensitive to the variation of the tide. Generally, tide plays an important role in the oceans such as mixing process, navigation, and tidal energy. Besides, the tidal flow is the main force of water circulation in the Yellow Sea. Therefore, it is necessary to predict accurately tidal elevation.

Over the 30 years, various tidal simulations for the Yellow Sea and the East China Sea have been conducted to understand the tide and tidal currents (An 1977; Bao et al. 2001; Choi 1980; Guo and Yanagi 1998; Kang et al. 1998; Lee and Jung 1998; Lefevere et al. 2000; Suh 2011; Yanagi and Inoue 1994). Most of the studies applied to finite-difference method. However, it had limitation to represent the complex geometry around the West Coast of Korea. To overcome

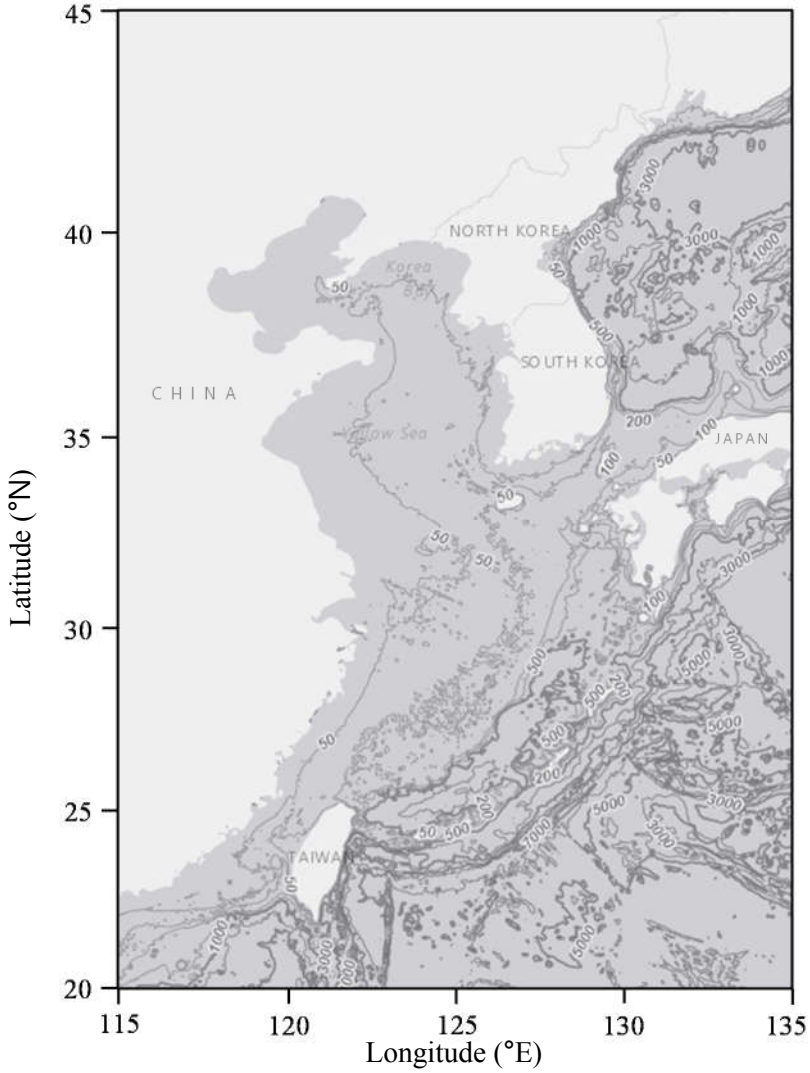

Figure 1. Geography and bathymetry configuration in the Yellow Sea and the East China Sea

this limitation, Lefevere et al. (2000) and Suh (2011) applied finite-element method and unstructured grid system in order to represent the complex geometry and improve the numerical result. However, there are a few studies about the tidal model for the Yellow Sea and the East China Sea using the unstructured grid system.

Along with representing the complex geometry, it is important to understand the effect of bottom friction and open boundary condition on the tidal model. Bottom friction highly influences tidal flow in shallow water. Therefore, accurate bottom friction would be required (Prandle, 1997; Lee et al., 2011) to obtain accurate tidal data through numerical simulation. Moreover, the bottom friction coefficient might be different depending on the regions because geographic characteristics are different. Furthermore, the open boundary condition influences the result of numerical simulation. Therefore, the accuracy of data for the open boundary condition is important in constructing the numerical model.

1.2 Necessity and Objective

1.2.1 Necessity

Numerical experiments in order to reproduce the tide in the Yellow Sea and the East China Sea mostly used observation data and tidal charts such as Ogura (1933) and Nishida (1980) for the open boundary conditions. However, there is some doubt about the accuracy of the data. Nowadays, several global or

regional tide models such as FES2014, TPXO9.1, NAO99, and NAO99Jb have been developed and distributed as digital data. The resolutions of the tide models are coarser along the coast and in the shallow water regions. Therefore, it is needed to construct a numerical model in order to obtain more detail tidal information in such regions. Furthermore, the open boundary conditions are important in the numerical model because the numerical results are sensitive depending on these conditions. Thus, it is necessary to find out the dependence of tidal elevation around the West Coast of Korea according to the open boundary conditions. The effect of the bottom friction should be reflected in the tidal flow because the bottom friction also highly affects tidal flow in shallow water. However, there is no global standard to determine the bottom friction coefficient, and the bottom friction coefficient should be determined based on local topography. The West Coast of Korea is surrounded by lots of islands including complex coastlines which also affect tidal elevation, so these effects should be considered in the numerical model.

1.2.2 Objective of this Study

The objective of this study was investigating the effect of bottom roughness and open boundary conditions on the tide around the West Coast of Korea through the numerical simulations in order to accurately obtain the tide information. To achieve this objective, firstly, various friction coefficients were applied to the numerical model to examine how the tide was changed depending on the values and the numerical results were calibrated and validated against

the observation data. Second, reproduced tides were examined through the numerical models applying three well-known tide models, FES2014, TPXO9.1 and NAO99Jb, as the open boundary conditions. Third, sensitivity analyses were carried out to find out the dependence of the tidal elevation on the variation of the open boundary conditions and characteristic of the tidal elevation around the West Coast of Korea.

CHAPTER 2. THEORETICAL BACKGROUND

2.1 Literature Review of Numerical Simulation of the Tide and Tidal Current in the Yellow Sea and the East China Sea

Numerous tidal simulations for the Yellow Sea and the East China Sea have been conducted, including both 2D model and 3D model.

Choi (1980) was the baseline of the tidal model for the Yellow Sea and the East China Sea. The seaward boundary was placed on the East China Sea, but the boundary was set at roughly 200 m isobaths to prevent the disturbance due to rapidly changing water depth. The study considered four constituents M2, S2, K1, and O1 obtained from Ogura chart (1933) and the co-tidal and co-range chart of each constituent were displayed. The study showed that 4-amphidrome system for the semidiurnal tide and a 2-amphidrome system for the diurnal tide.

Yanagi and Inoue (1994) studied tidal flow using 2D finite-difference model on a β-plane with 25km x 25km grid size. The study considered five major constituents, M2, S2, N2, K1, and O1, and 0.0026 was applied for the bottom friction coefficient. The results were compared with Choi (1980) and observation data. The results were similar to Choi (1980).

Kang et al. (1998) examined the tidal regimes of M2, S2, N2, K1, and O1. In addition, this study investigated M4 and MS4 tidal regimes that were generated through nonlinear interaction by M2 and S2. The study constructed fine grid

system at 1/16° in latitude and 1/12° in longitude. Non-constant values and constant value of the friction coefficient based on the Chezy coefficient were applied to the numerical model. The observation data were used for the open boundary condition and validated numerical results. The numerical results showed good agreement with the observation data. In M2 case, the RMS of amplitude was 9.7 cm, and RMS of phase was 4.5°. However, in the case of M4 and MS4, there were relatively large deviations between the observation data and the numerical results, especially near the Kyunggi Bay. The geometry of the Kyunggi Bay was complicated, but the model didn't consider geometry effect sufficiently.

Lefevre et al. (2000) investigated the way that how to improve the tidal model. The study chose the Yellow Sea and the East China Sea for a test area because the accuracy of FES94.1 solution for the Yellow Sea and the East China Sea was poor rather than other shelf areas. Finite-element method was applied to the tidal model with refined the mesh and different 9 values of friction coefficient were applied to the computation domain respectively in order to evaluate the sensitivity of the model to the bottom friction. The accuracy of the results was higher than 90% of M2, K1, O1 however, the accuracy of the result of S2 is relatively low because the data quality of S2 for boundary condition was not good.

Guo and Yanagi (1998) examined the vertical distribution of tidal current using a 3D model with high horizontal resolution (12.5 km) and the vertical (20

layers). Major four tidal constituents, M2, K1, S2, and O1, were considered and cotidal chart by Nishida (1980) was used to the open boundary conditions. Through various simulation case with different sea bed drag coefficients, the sensitivity of the tidal current depending on the drag coefficients was examined.

Lee and Jung (1999) applied to 3D finite-difference model with four eddy viscosity closure models. The study examined the influence of the bottom friction coefficient upon tide amplitude and tidal current of M2. The model results were compared with selected observation data. The study revealed that the optimal value of bottom friction coefficient changes sensitively according to the eddy viscosity formulations.

BAO et al. (2000) carried out 3D numerical simulation with fine horizontal resolution (5' x 5') and vertical (15 levels) grids and considered four constituents, M2, S2, K1, and O1. Nonuniformity values of the bottom friction coefficient by the empirical formulation in depth-dependent form. The numerical results were in good agreement with observation data for tidal elevation and tidal currents.

Lu and Zhang (2006) used the adjoint model to find the optimal value of the bottom friction coefficient depend on the regions in the Yellow Sea and the East China Sea. T/P altimeter data were assimilated into a 2D adjoint tidal model to optimizing the bottom friction coefficients depend on the space. The tidal elevations were sensitive to bottom friction coefficient near the land and less sensitive to the bottom friction coefficient in the middle ocean.

2.2 Model Description

Telemac-2D was used as a CFD tool for numerical simulation of the tidal flow in the Yellow Sea and the East China Sea. It is an open-source CFD program developed by the Research and Development Department of Electricité de France (EDF). It deals with the solution of depth-averaged Navier-Stokes equations and it uses high capacity algorithms based on the finite-element method. Space is discretized in the form of an unstructured grid of triangular elements, and it is also possible to deal with quadrilateral elements. That means that it can be refined particularly in areas of special interest.

2.2.1 Numerical Model Equations

Shallow Water equations which are derived from Navier-Stokes equations by integration from the bottom to the surface are set of equations in Telemac-2D with certain hypotheses. The main restrictive assumption that has to be made is that the horizontal length scale is much larger than the vertical length scale.

2.2.1.1 Hypotheses, Approximations and Calculation Rules

Hydrostatic pressure

The pressure is assumed to be hydrostatic that is the pressure being due to the weight of the column of water above the coordinates (x, y, z).

$$\frac{\partial p}{\partial z} = -\rho g \text{ that is } p(x, y, z) = -\rho g z + const$$

at the bottom $p = \rho g h$

Negligible vertical velocity

Vertical velocity is negligible in the Shallow Water equation and will not have an equation.

Impermeability of the surface and the bottom

There is no transfer of water mass through the surface and the bottom.

2.2.1.2 Shallow Water Equations

The Navier-Stokes equations with constant density and hydrostatic pressure are averaged vertically by integrating from the bottom to the surface. The Shallow Water equations become as follows.

Continuity Equation

$$\frac{\partial h}{\partial t}+\frac{\partial (hu)}{\partial x}+\frac{\partial (hv)}{\partial y}=0$$

Momentum equations

$$\frac{\partial (hu)}{\partial t}+\frac{\partial}{\partial x}(huu)+\frac{\partial}{\partial y}(huv)=-gh\frac{\partial Z_s}{\partial x}+hF_x+div(h\nu_e\overrightarrow{grad}(u))$$

$$\frac{\partial (hv)}{\partial t}+\frac{\partial}{\partial x}(huv)+\frac{\partial}{\partial y}(hvv)=-gh\frac{\partial Z_s}{\partial y}+hF_y+div(h\nu_e\overrightarrow{grad}(v))$$

where
h : water depth
u, v: velocity component
Z_s : free surface elevation
F : coriolis force
ν_e : effective diffusion(turbulent viscosity and dispersion)

Two new variables as follows are appeared during averaging vertically of horizontal components of the three-dimensional velocity vector.

$$u = \frac{1}{h}\int_{Z_f}^{Z_s} U dz \text{ and } v = \frac{1}{h}\int_{Z_f}^{Z_s} V dz$$

Dispersion term appears during the integration of the advection term from the bottom to the water surface. The dispersion term can be described as additional diffusion and these terms are not zero when there are heterogeneities of velocity vertically.

$$\frac{1}{h}\frac{\partial}{\partial x}\int_{Z_f}^{Z_s} u'' u'' dz + \frac{1}{h}\frac{\partial}{\partial y}\int_{Z_f}^{Z_s} u'' v'' dz$$
$$\frac{1}{h}\frac{\partial}{\partial x}\int_{Z_f}^{Z_s} u'' v'' dz + \frac{1}{h}\frac{\partial}{\partial y}\int_{Z_f}^{Z_s} v'' v'' dz$$

In order to take account the dispersion terms, these terms are modified to viscosity or turbulent viscosity and replace it by an effective viscosity integrating the dispersion phenomenon. Effective diffusion term, ν_e, in above momentum equations explains both turbulent viscosity and dispersion.

2.2.2 Bottom Friction

The bottom shear stress acting on the fluid is opposed to the fluid velocity. For tidal modeling, the effect of the bottom shear stress becomes prominent, especially near the coastlines and shallow water. The bottom shear stress can be expressed with dimensionless friction coefficient, C_f.

$$\tau_{bx} = -\frac{u}{2}\rho C_f \sqrt{u^2 + v^2}$$

$$\tau_{by} = -\frac{v}{2}\rho C_f \sqrt{u^2 + v^2}$$

However, the friction coefficient, C_f, is an unknown parameter. This is why calibrating the numerical model is important, and understating of the effect of bottom friction on numerical results is important.

2.2.3 Coriolis Force

Coriolis force is occurred by the rotation of the Earth on its own axis. Coriolis force can be considered as constant across small areas. However, when the computation domain covers large areas, the Coriolis force should be varied spatially. Coriolis force is expressed as below formula in 2-dimensions.

$$F_x^c = 2\omega \sin(\lambda) v = fv$$
$$F_y^c = -2\omega \sin(\lambda) u = -fu$$

where

ω: angular velocity of the Earth ($7.292 \times 10^{-5} rad / s$)

λ: latitude

2.2.4 Turbulence Modeling (*k-ε* model)

Reynolds stresses which are the additional terms appear during averaging of the Navier-Stokes equations over time. Reynolds stresses corresponding to the transport of momentum due to the turbulent fluctuation in physically. Turbulence closure model is necessary to determine the Reynolds stress terms.

In this study, extension of the classical *k*- ε model was adapted to the Saint-Venant equations to take account of the dispersion terms. The *k*-ε model is one of the turbulence model, which explains the turbulence with turbulent kinetic energy (*k*) and turbulent dissipation (ε).

The vertically averaged values of *k* and ε are

$$k = \frac{1}{h}\int_{Z_f}^{Z_s} \frac{1}{2}\overline{u_i' u_j'}\, dz$$

$$\varepsilon = \frac{1}{h}\int_{Z_f}^{Z_s} \nu \overline{\frac{\partial u_i'}{\partial x_j}\frac{\partial u_i'}{\partial x_j}}\, dz$$

where u_i' : turbulent fluctuation of velocity

These *k* and ε equations take the form as follows.

$$\frac{\partial k}{\partial t} + u_i \frac{\partial k}{\partial x_i} = \frac{1}{h} div\left(h \frac{\nu_t}{\sigma_k} \overrightarrow{grad}(k) \right) + P - \varepsilon + P_{kv}$$

$$\frac{\partial \varepsilon}{\partial t} + u_i \frac{\partial \varepsilon}{\partial x_i} = \frac{1}{h} div\left(h \frac{\nu_t}{\sigma_\varepsilon} \overrightarrow{grad}(\varepsilon) \right) + \frac{\varepsilon}{k}[C_{1\varepsilon} P - C_{2\varepsilon}\varepsilon] + P_{\varepsilon v}$$

The production terms are calculated with horizontal velocity gradients.

$$P = \nu_t \left(\frac{\partial u_i}{\partial x_j} + \frac{\partial u_j}{\partial x_i} \right) \frac{\partial u_i}{\partial x_j}$$

where $\nu_t = C_\mu \frac{k^2}{\varepsilon}$

P_{kv} and $P_{\varepsilon v}$ are due to the shear force of flow along the vertical.

$$P_{kv} = C_k \frac{u_*^3}{h} \text{ and } P_{\varepsilon v} = C_\varepsilon \frac{u_*^4}{h^2}$$

where

$$u_* = \sqrt{\frac{C_f}{2}(u^2 + v^2)}$$

$$C_k = \frac{1}{\sqrt{C_f}}$$

$$C_\varepsilon = 3.6 \frac{C_{2\varepsilon}\sqrt{C_\mu}}{C_f^{3/4}}$$

The constants such as $C_{1\varepsilon}$, $C_{2\varepsilon}$, σ_k, and σ_ε of the *k*-ε model have been determined by comparison with a simple case. And the friction coefficient, C_f, is deduced from the chosen friction law in the numerical model.

2.2.5 Boundary Condition

The physical boundary plays important role in the numerical simulation. In an aspect of the physics, the boundary should be distinct between solid boundary and liquid boundary.

Solid boundary

There is no flow in normal direction, and the boundary is an impermeable condition.

Liquid boundary

Liquid boundary supposes the existence of a fluid domain, but it does not belong to the domain of calculation. However, liquid boundary highly influences the calculation.

2.3 Tide

Tides are the rise and fall of the water level on the ocean within several meters caused by combined effects of the gravitational forces exerted by the moon and the sun, and the rotation of the earth. Tides are commonly classified as semi-diurnal, diurnal or mixed based on the number of high and low water level and relative water heights. Semi-diurnal tides have nearly two equal high water level and two equal low water level in a lunar day (about 24hr 50min). Diurnal tides have one high water level and low water level each lunar day. If two unequal high water level and two unequal low water level occur per lunar day, it is called mixed tide. It is noticeably that over-tides and compound tides are produced during propagation of the tides into the shallow water, and the shape of the tides is changed.

The height range of semi-diurnal tides varies in the two-week cycle when M2 and S2 tides are combined. When the earth, the moon, and the sun lie approximately in the same line, lunar tide and solar tide coincide. In that time, an amplitude of the tide is the greatest. This called spring tide. On the other hand, between the spring tide after the first and third quarter, an amplitude of the tide is lowest. This called neap tide.

The water level due to tides can be described in terms of harmonic terms.

$$h = S_0 + \sum_i h_i \cos(\omega_i t + \alpha_i)$$

where

S_0 : height of the mean water level above the datum

h_i : amplitudes of each tidal constituents

ω_n : frequency of each tidal constituents

α_n : phase of each tidal constituents

Amplitude and phase of each tidal constituent are greatly varied in spatially. On the other hand, frequency for each tidal constituent is constant everywhere. Therefore, amplitude and phase for each tidal constituent which has unique frequency can be determined using harmonic analysis. In this study, harmonic constants of each tidal constituent were calculated using T_TIDE (Pawlowicz et al., 2002).

2.4 Tide Model

Recently, sea surface height data can be measured accurately. Based on this data, several assimilation tide models with highly accurate data have been developed, such as global ocean tide models, FES2014, NAO99 and TPXO9.1, and regional ocean tide model, NAO99Jb. FES2014 was produced by Noveltis, Legos, and CLS and distributed by Aviso+, with support from Cnes (https://www.aviso.altimetry.fr/). The FES2014 has been constructed based on the dynamic model (T-UGO model), data analysis, and assimilation. The gridded resolution of the data package is 1/16°. NAO99 with 1/2° grid resolution was constructed based on 5 years of TOPEX/POSEIDON altimeter

data and barotropic hydrodynamic model. High-resolution regional ocean tide model NAO99Jb was also developed based on both TOPEX/POSEIDON data and 219 coastal tide gauges data. Tidal data from NAO99Jb can be applied to the tidal model for the Yellow Sea and the East China Sea because NAO99Jb covers from 110°E to 165°E and from 20°N to 65°N. NAO99 and NAO99Jb can be downloaded from the website (https://www.miz.nao.ac.jp/staffs/nao99/index_En.html). TPXO9.1 has been developed based on least-square sense, the Laplace tidal equation, and altimetry data. The distributed TPXO9.1 data has 1/6° resolution. The data can be downloaded from the website (http://volkov.oce.orst.edu/tides/)

The accuracy of the ocean tide models has been improved, including shallow water area by obtaining accurate observation data and using data assimilation method. However, the data accuracy in the Yellow Sea and the East China Sea still lower than in other areas. The tidal data from the tide models are compared with observation data obtained from 23 tide station along the West Coast of Korea (Figure 2 and Table 1). The observation data in each tide station can be downloaded from the Korean Hydrographic and Oceanographic Agency (KHOA, http://www.khoa.go.kr/koofs/eng/observation/obs_real.do). From the downloaded time series tide data, tidal harmonic constants of each tidal constituent were computed and compared with the ocean tide model data (FES2014, NAO99, NAO99Jb, and TPXO9.1). The RMSE of four major constituents is indicated in Table 2. The RMSE for M2 amplitude which is the

most dominant tidal constituent around the West Coast of Korea was over 20 cm except NAO99Jb. The difference between observation data and tidal model data in the Yellow Sea and the East China Sea was a bit larger than the mean RMSE for M2 of the ocean tide models in the deep ocean and shelf seas which is less than 10cm (Matsumoto et al. 2000; Carrere et al. 2012). Especially, the difference between the observation data and the tide model data is large in Incheon region in case of M2 and S2. In addition, RMSEs of K1 and O1 are high considering the range of these amplitudes.

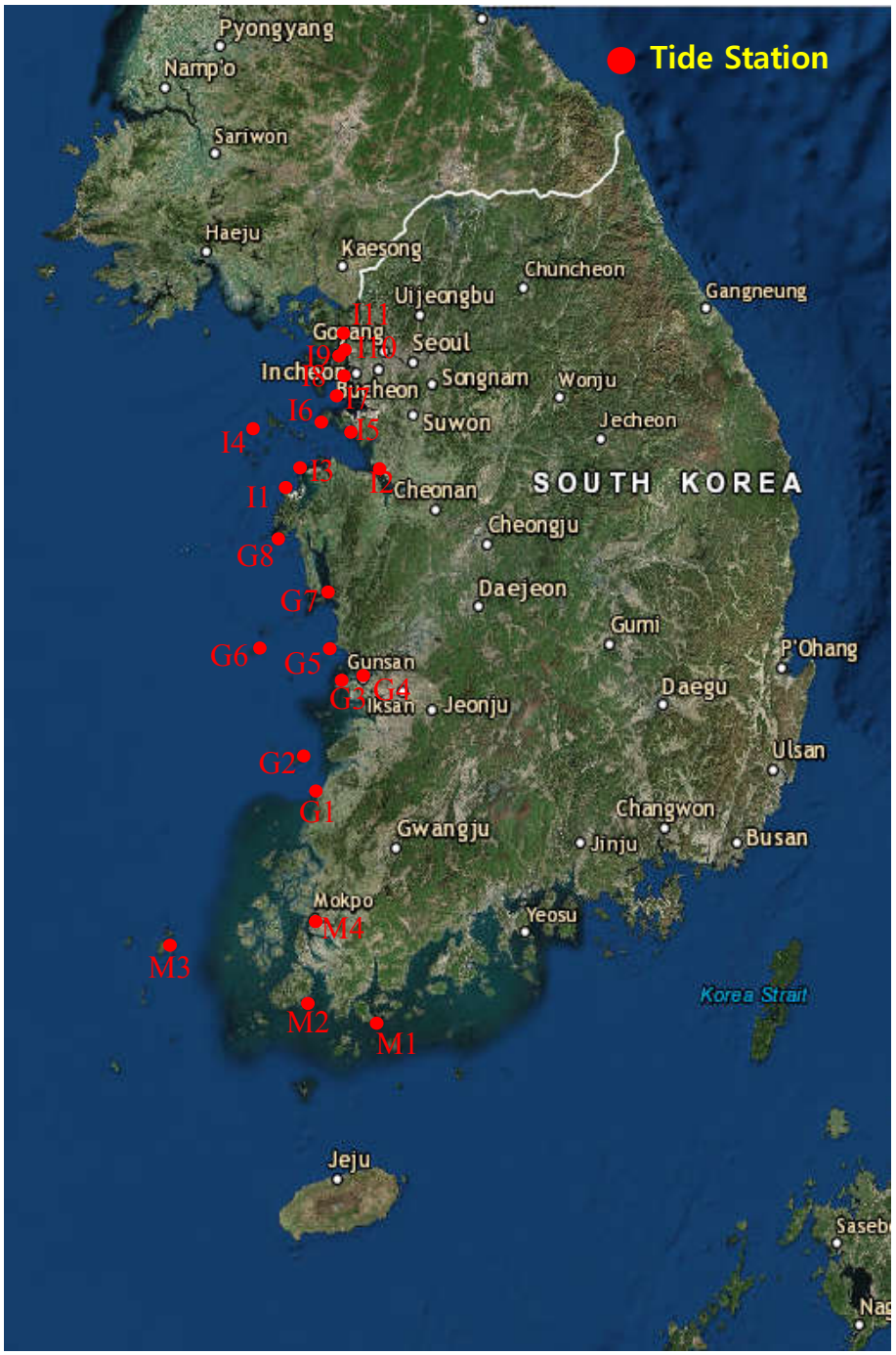

Figure 2. Location of the tide stations along the West Coast of Korea

Table 1. Name and location of the tide stations along the West Coast of Korea

Station No.	Station Name	Latitude (°N)	Longitude (°E)	Region
M1	Wando	34.3	126.8	Mokpo
M2	Jindo	34.4	126.3	Mokpo
M3	Heuksando	34.7	125.4	Mokpo
M4	Mokpo	34.8	126.4	Mokpo
G1	Yeonggwang	35.4	126.4	Gunsan
G2	Wido	35.6	126.3	Gunsan
G3	Gunsan	36.0	126.6	Gunsan
G4	Janghang	36.0	126.7	Gunsan
G5	Eocheongdo	36.1	126.0	Gunsan
G6	Seocheonmaryang	36.1	126.5	Gunsan
G7	Boryeong	36.4	126.5	Gunsan
G8	Anheung	36.7	126.1	Incheon
I1	Taean	36.9	126.2	Incheon
I2	Pyeongtaek	37.0	126.8	Incheon
I3	Daesan	37.0	126.4	Incheon
I4	Ansan	37.2	126.6	Incheon
I5	Gureopdo	37.2	126.0	Incheon
I6	Yeongheungdo	37.2	126.4	Incheon
I7	IncheonSongdo	37.3	126.6	Incheon
I8	Incheon	37.5	126.6	Incheon
I9	Yeongjongbridge	37.5	126.6	Incheon
I10	Gyeongin	37.6	126.6	Incheon
I11	Ganghwa	37.7	126.5	Incheon

Table 2. RMSE between the observation data and the tide models

Tide Model	Resolution	M2		K1		S2		O1	
		Amp (cm)	Phase (°)	Amp (cm)	Phase (°)	Amp (cm)	Phase (°)	Amp (cm)	Phase (°)
FES2014	1/16°	20.2	8.2	4.2	5.4	14.6	10.9	3.8	11.0
NAO99Jb	1/12°	16.1	5.4	4.9	7.6	8.4	8.8	4.8	31.8
NAO99	1/2°	34.0	16.6	6.4	8.0	16.5	12.8	5.6	7.1
TPXO9.1	1/6°	25.0	6.6	6.2	7.5	11.4	7.1	3.9	6.1

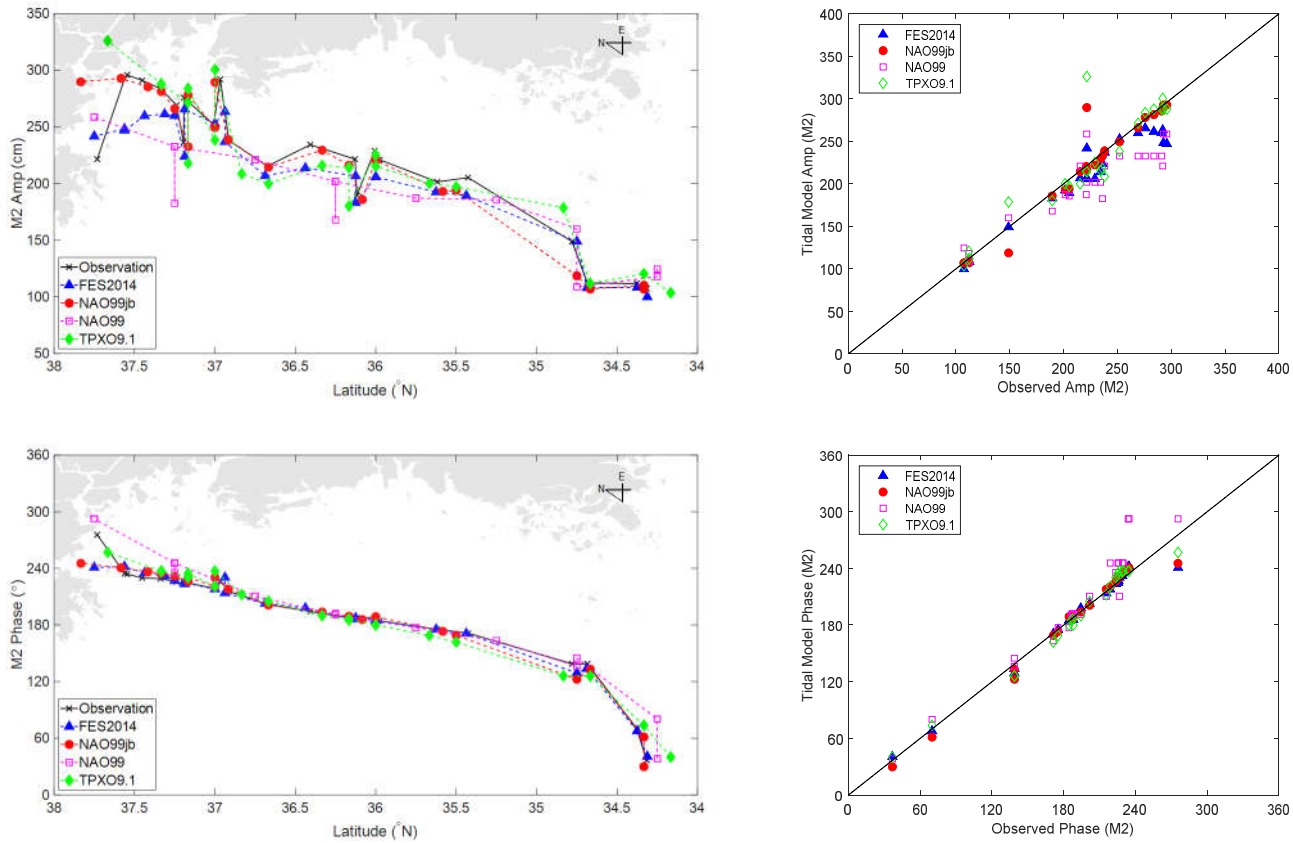

Figure 3. Comparison between the observation data and the tide model data of M2 tidal constituent

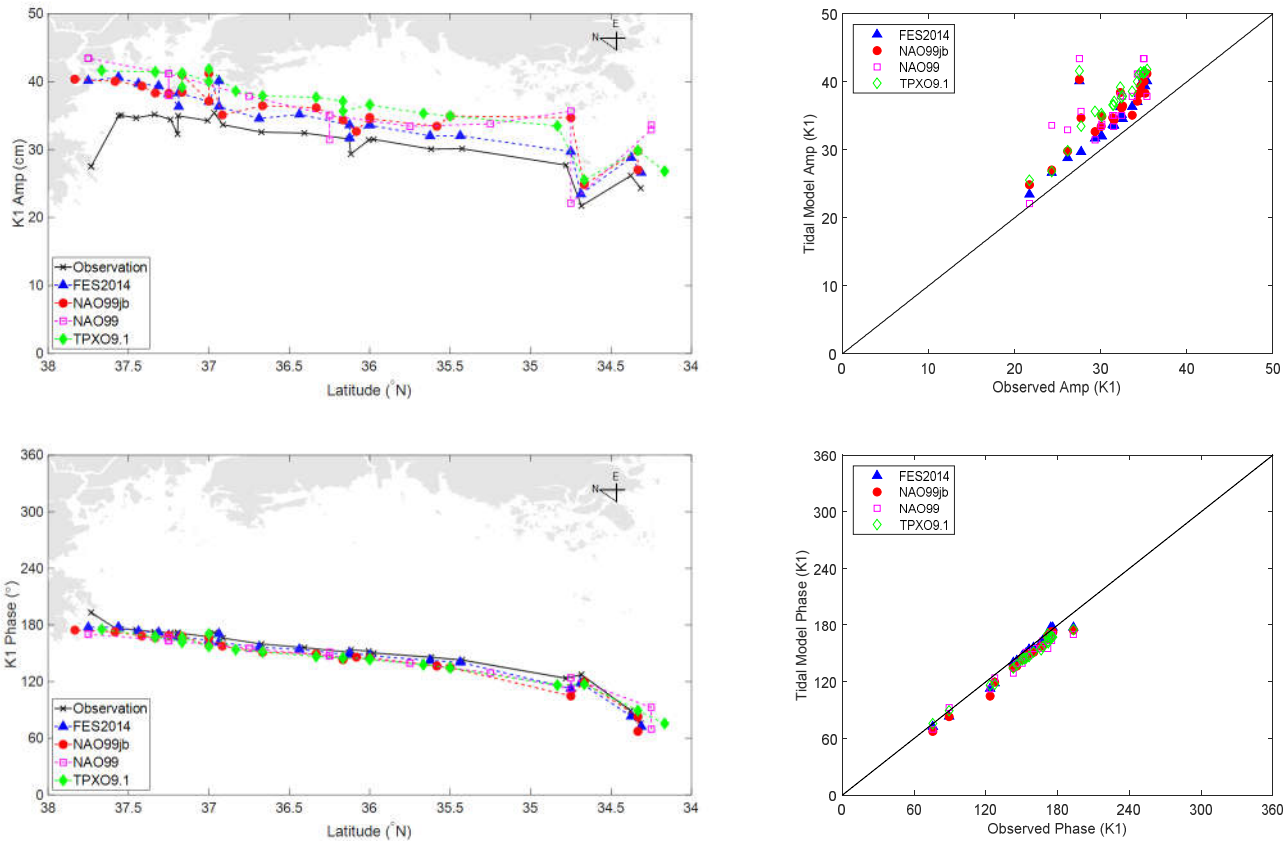

Figure 4. Comparison between the observation data and the tide model data of K1 tidal constituent

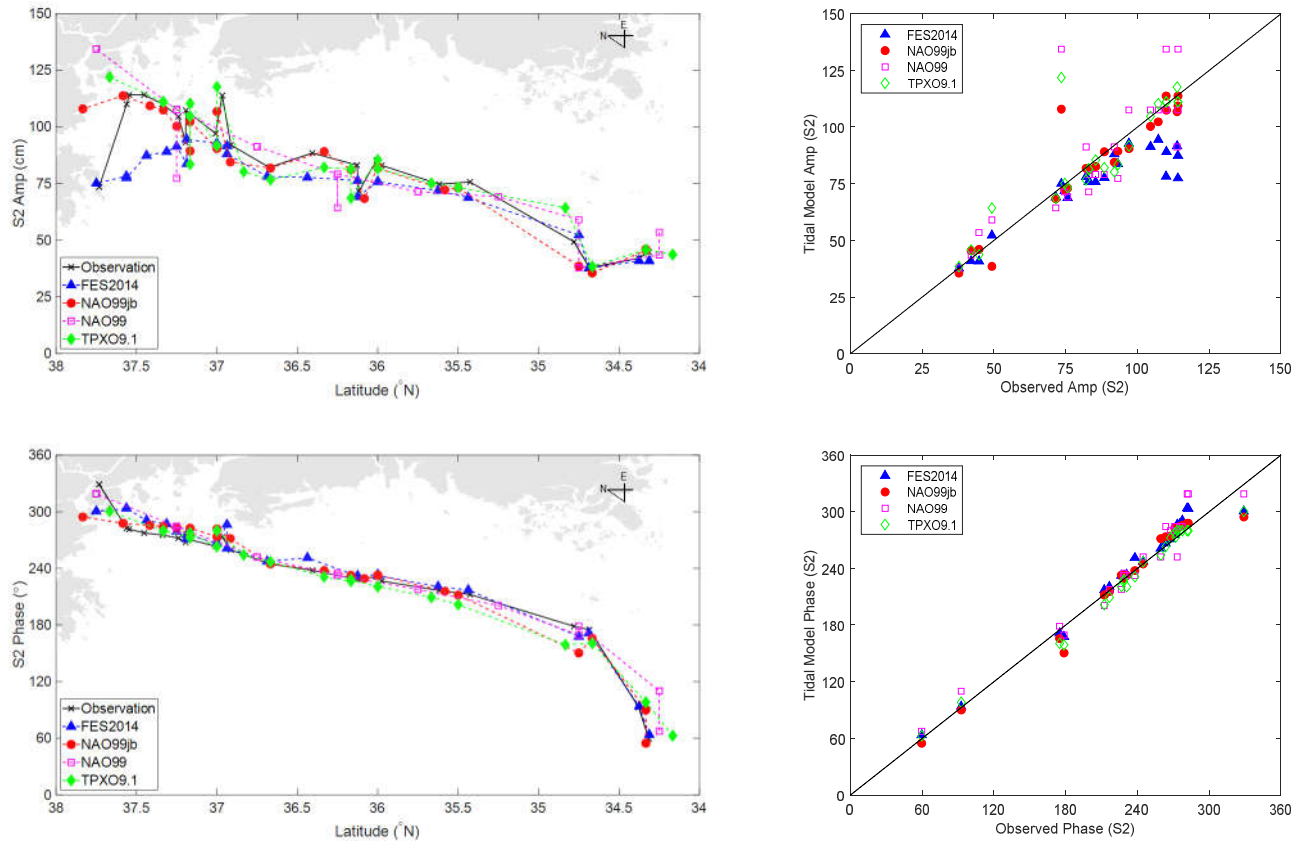

Figure 5. Comparison between the observation data and the tide model data of S2 tidal constituent

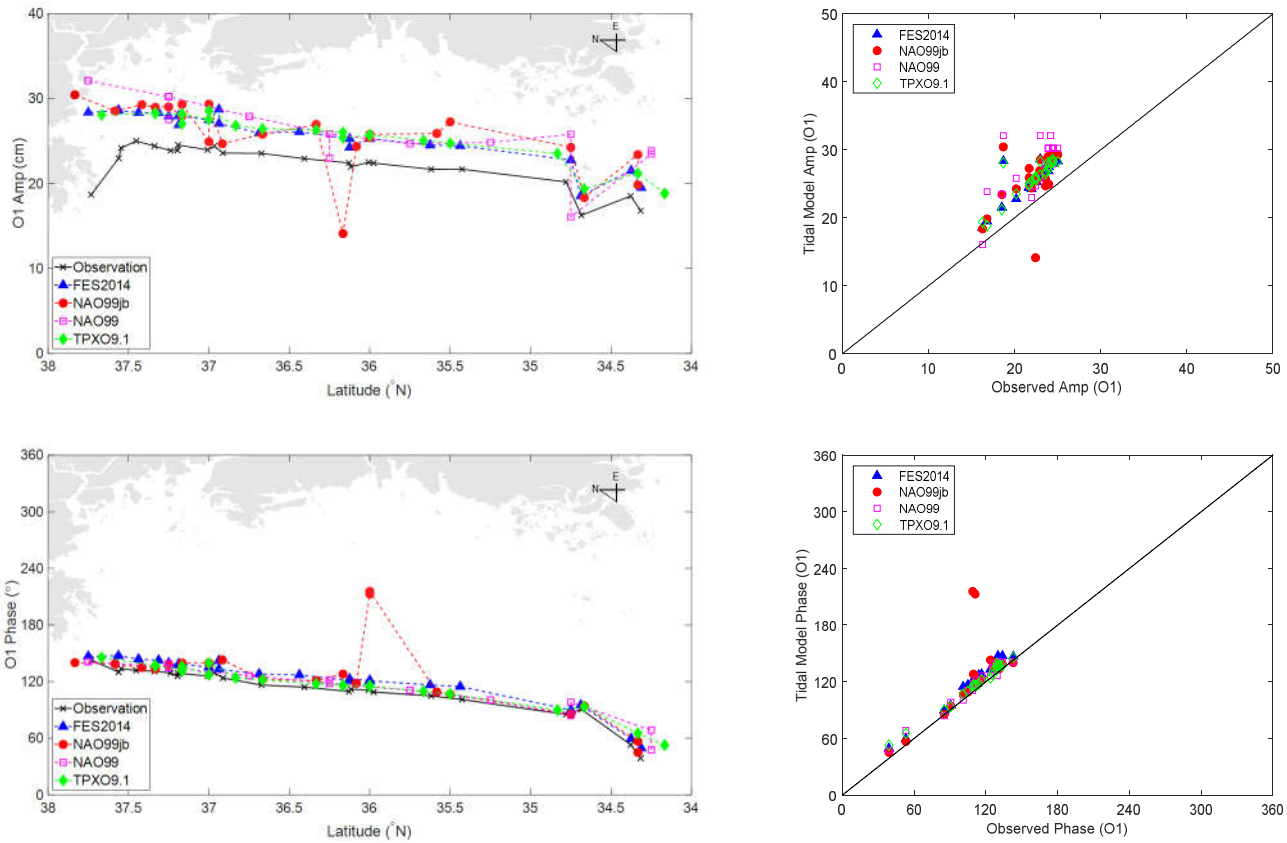

Figure 6. Comparison between the observation data and the tide model data of O1 tidal constituent

CHAPTER 3. METHODOLOGY

3.1 Computation Domain

The computation domain used in this study covered from 24°N up to 41°N in latitude and from 17.5°E up to 131°E in longitude. The open boundaries placed on Taiwan Strait, Okinawa Through and Korean Strait (Figure 7). The main flow was running from Taiwan Strait, Okinawa Through and Korean Strait and the flow were going through the East China Sea, the Yellow Sea, and reaching to the Bohai Sea. The Okinawa Through is placed on the continental shelf with a dramatic change in water depth. For that reason, the open boundary lines should be carefully determined.

The computation domain was created by unstructured grid system with different horizontal resolution using BlueKenue, which is the pre-processing and post-processing program of the Telemac-2D. The geometry adjacent to the coastline along the West Coast of Korea is very irregular and there are lots of small islands. Thus, in that region, the computation grids consisted of a very fine grid that the default value was 1/100° in order to represent complex geometry. The grids for other coastal area were created with default value 1/24°, and relatively coarse grid about 1/12° was used to form the interior of the Yellow Sea and the East China Sea (Figure 8). GEBCO2014 with 1 min resolution was used to bathymetry data for the computation domain. (https://www.ngdc.noaa.gov/mgg/ibcm/ibcmdvc.html).

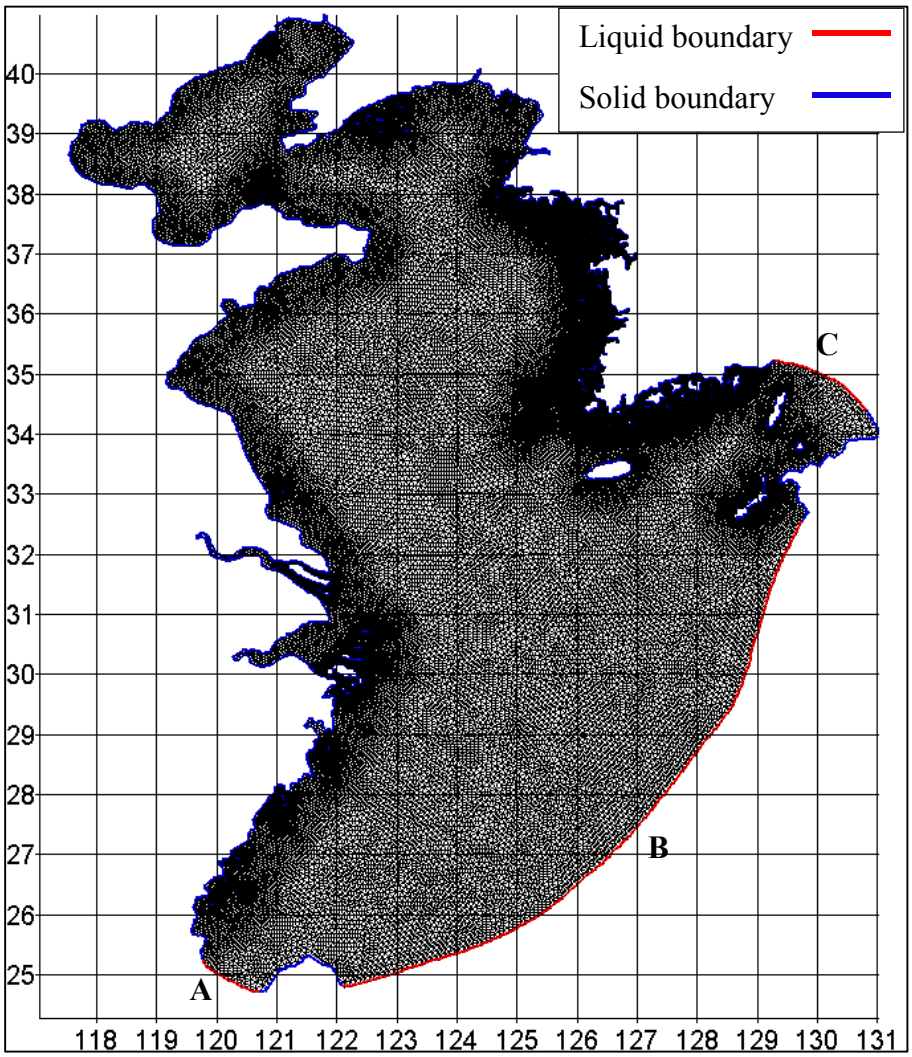

Figure 7. Liquid boundary and solid boundary in the computation domain

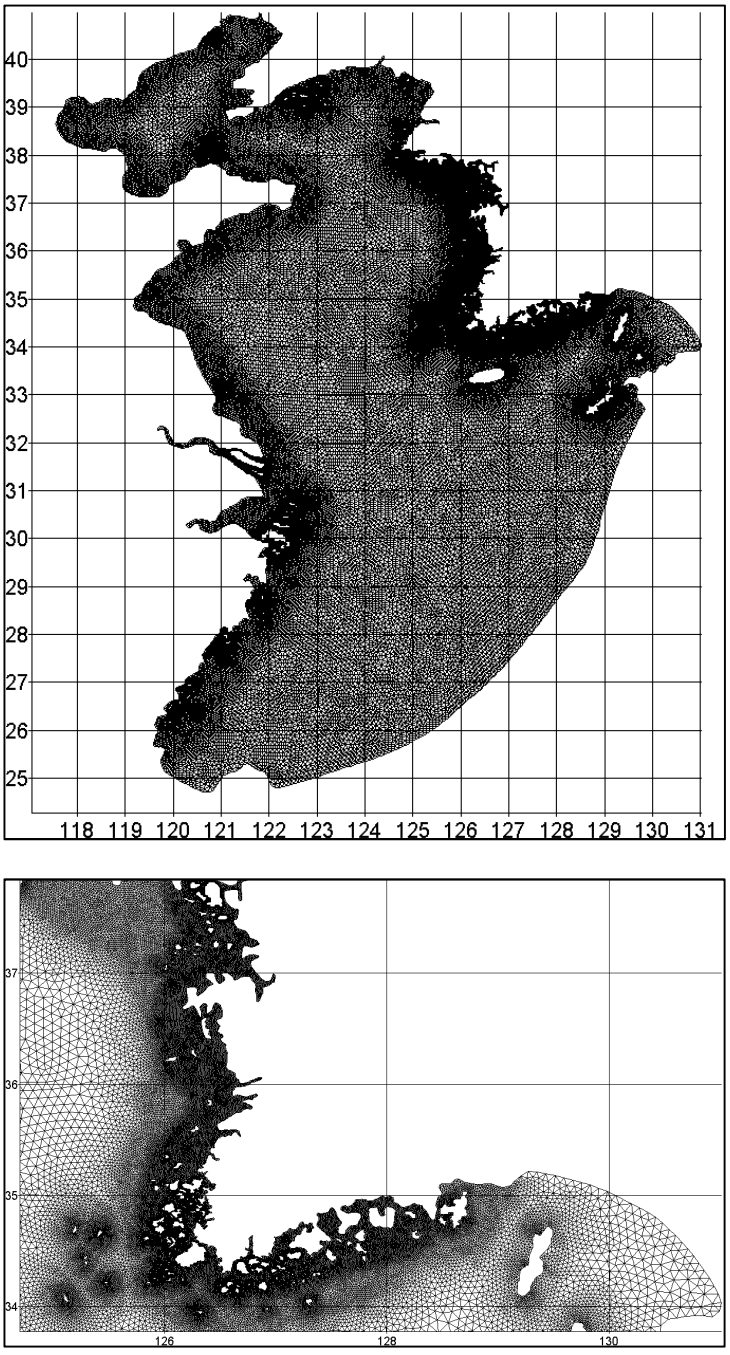

Figure 8. Horizontal unstructured grid of the Yellow Sea and the East China Sea and an enlarging of the West Coast of Korea

3.2 Boundary Condition

At the seaward open boundaries, water elevations were specified to simulate tidal flow. The elevation of the water surface was determined using the below formula.

$$H = \sum H_i$$

where

$$H_i(M,t) = A_{F_i}(M)\cos\left(2\pi\frac{t}{T} - \varphi_{F_i}(M)\right)$$

A_{F_i} : *amplitude of the height of each tidal constituent*

T : *period of each tidal constituent*

φ_{F_i} : *phase of each tidal constituent*

The H_i is the water elevation of each tidal constituent. The summation of each water elevation was applied to each node on the open boundary. In this study, four major tidal constituents, M2, S2, K1, and O1, were considered and the harmonic constants of the tidal constituents for the open boundary conditions were obtained from global and regional tide models, FES2014, NAO99Jb and TPXO9.1.

Other boundaries except the seaward open boundaries were set as the solid boundary. The boundary conditions were shown in Figure 7.

3.3 Bottom Friction

The quadratic bottom friction law was used to describe the bottom friction. There is no global standard for computing bottom friction coefficient, C_f. The optimum value of bottom friction coefficient is different depending on regions.

In previous studies, the bottom friction coefficient was usually taken from 0.0015 to 0.003. Five different bottom friction coefficients were uniformly applied to the whole computation domain respectively and then how the tide changes were examined depending on the bottom friction coefficient along the West Coast of Korea. Table 3 showed the simulation cases including the values of bottom friction coefficient and tide models for the open boundary conditions.

Table 3. Simulation cases with the uniform bottom friction coefficient

Case	Tide Model	Friction Coefficient
FES 1-1	FES2014	0.0015
FES 1-2	FES2014	0.002
FES 1-3	FES2014	0.0023
FES 1-4	FES2014	0.0025
FES 1-5	FES2014	0.003
NAO 1-1	NAO99Jb	0.0015
NAO 1-2	NAO99Jb	0.002
NAO 1-3	NAO99Jb	0.0023
NAO 1-4	NAO99Jb	0.0025
NAO 1-5	NAO99Jb	0.003
TPX 1-1	TPXO9.1	0.0015
TPX 1-2	TPXO9.1	0.002
TPX 1-3	TPXO9.1	0.0023
TPX 1-4	TPXO9.1	0.0025
TPX 1-5	TPXO9.1	0.003

Different values of bottom friction coefficient should be required in different regions because of geographic characteristics. The bottom slope is relatively milder in Incheon region than Mokpo region and Gunsan region, and there are lots of islands around Mokpo region rather than Incheon region. Therefore, it can be expected that more energy dissipated in Mokpo region and Gunsan

region than Incheon region. For that reason, different values of the bottom friction coefficient were applied to three regions. The simulation cases were shown in Table 4 including the tide models and bottom friction coefficient depending on the regions.

Table 4. Simulation cases with different bottom friction coefficient depending on the regions

Case	Tide Model	Friction Coefficient		
		Mokpo	Gunsan	Incheon
FES 2-1	FES2014	0.0025	0.0027	0.002
FES 2-2	FES2014	0.0025	0.003	0.002
FES 2-3	FES2014	0.0025	0.0035	0.0018
FES 2-4	FES2014	0.0025	0.0035	0.002
NAO 2-1	NAO99Jb	0.0025	0.0027	0.002
NAO 2-2	NAO99Jb	0.0025	0.003	0.002
NAO 2-3	NAO99Jb	0.0025	0.0035	0.0018
NAO 2-4	NAO99Jb	0.0025	0.0035	0.002
TPX 2-1	TPXO9.1	0.0025	0.0027	0.002
TPX 2-2	TPXO9.1	0.0025	0.003	0.002
TPX 2-3	TPXO9.1	0.0025	0.0035	0.0018
TPX 2-4	TPXO9.1	0.0025	0.0035	0.002

CHAPTER 4. RESULTS

4.1 Tidal Elevation

This study focused on the tidal wave propagation around the West Coast of Korea. The model results were validated with observation data collected from the 23 tide stations along the West Coast of Korea (Figure 2).

The simulation results classified into three regions, which were Mokpo region, Gunsan region, and Incheon region according to the location of the tide stations and the results were evaluated with RMSE by regions.

$$RMSE = \sqrt{(a_{o,i} - a_{s,i})^2 / N}$$

where

$a_{o,i}$: observed amplitude at i-th tide station point

$a_{s,i}$: amplitude from the simulation result at i-th tide station point

N : number of total tide station

The RMSE of the numerical results were shown in Table 5, Table 6, and Table 7 corresponding to the tide models. Comparison of amplitude and phase of each tidal constituent between the observation data and numerical results were shown in Figure 9 to Figure 20. The numerical results for the amplitude of M2 which were most dominant tide around the West Coast of Korea were in good agreement when the values of the bottom friction coefficient were from 0.002 to 0.0025. The most appropriate value of bottom friction coefficient was 0.0023 if the value is uniformly applied to the whole computation domain. The results for other tidal constituents, K1, S2, and O1, also were in good agreement when

the bottom friction coefficient was 0.0023. However, there was a limitation to reproduce M2 tide by applying bottom friction coefficient uniformly to the whole computation domain. It was noticed some areas where were a relatively large difference between the observation data and the simulation results for M2.

Simulation results from the model applying different values of bottom friction coefficient depending on the regions were in good agreement with the observation data rather than the results obtained from the model with an uniform bottom friction coefficient. The computed amplitudes of M2 for Gunsan region and Incheon region were improved. The minimum RMSE for M2 was 15.16 cm computed from the simulation case TPX 1-3 and 12.45 cm computed from the simulation case TPX 2-1. The results were shown in Table 8 and Figure 21.

Table 5. RMSE compared between the observation data and the computed amplitudes (FES2014)

Ocean Tide Model	Tidal Consitituent	C_f	RMSE (cm)			
			Mokpo (M)	Gunsan (G)	Incheon (I)	Mean
FES2014	M2	0.0015	18.97	34.83	40.18	35.45
		0.002	18.64	22.87	16.62	19.35
		0.0023	18.12	16.49	14.39	15.83
		0.0025	17.70	12.99	19.28	17.06
		0.003	17.38	10.58	35.57	26.39
	K1	0.0015	0.96	1.46	2.07	1.72
		0.002	0.93	1.30	2.03	1.64
		0.0023	0.95	1.48	2.34	1.88
		0.0025	1.00	1.70	2.64	2.12
		0.003	1.20	2.35	3.51	2.84
	S2	0.0015	8.49	10.94	12.21	11.20
		0.002	7.96	6.92	19.21	14.29
		0.0023	7.88	6.24	23.41	16.92
		0.0025	7.72	6.59	26.12	18.75
		0.003	7.66	8.99	31.90	22.91
	O1	0.0015	1.01	1.71	1.33	1.43
		0.002	1.32	2.38	1.86	1.99
		0.0023	1.45	2.67	2.26	2.30
		0.0025	1.54	2.86	2.53	2.52
		0.003	1.80	3.38	3.27	3.11

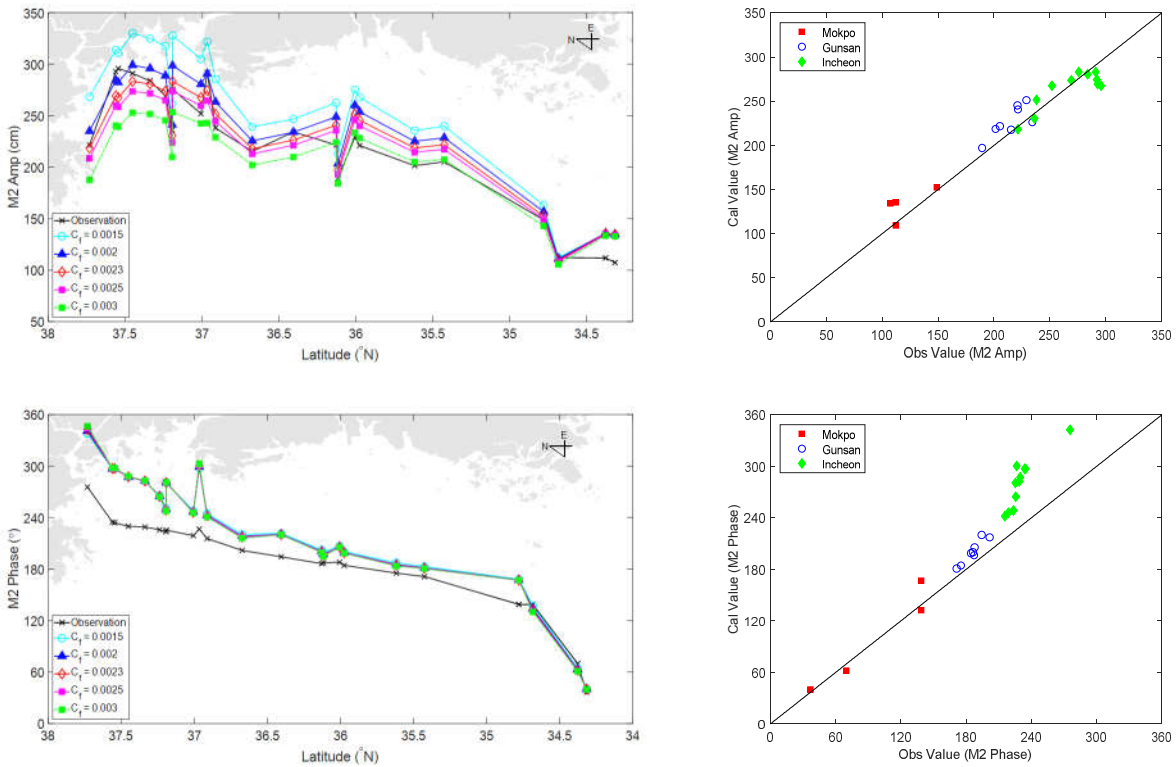

Figure 9. Comparison between the observation data and the computed amplitudes and phase of M2 corresponding to bottom friction coefficient (left) and Comparison between the observation data and the computed amplitudes and phase of M2 with bottom friction coefficient 0.0023 (right)

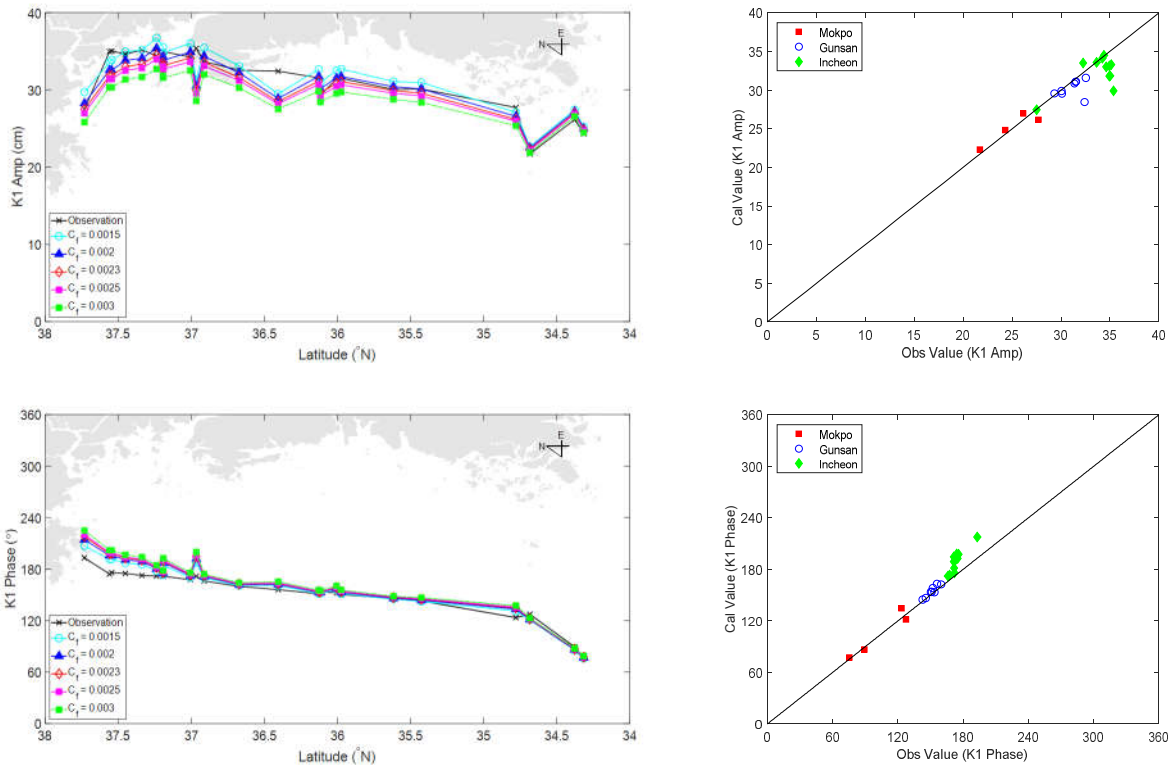

Figure 10. Comparison between the observation data and the computed amplitudes and phase of K1 corresponding to bottom friction coefficient (left) and Comparison between the observation data and the computed amplitudes and phase of K1 with bottom friction coefficient 0.0023 (right)

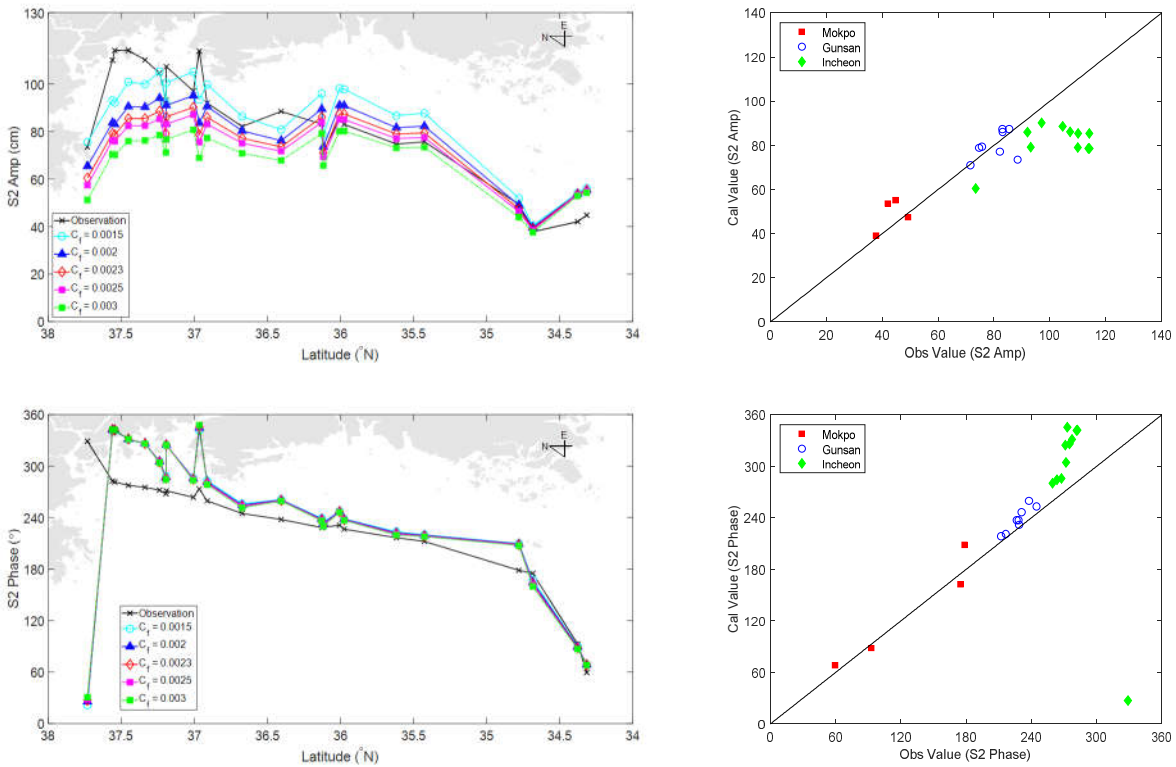

Figure 11. Comparison between the observation data and the computed amplitudes and phase of S2 corresponding to bottom friction coefficient (left) and Comparison between the observation data and the computed amplitudes and phase of S2 with bottom friction coefficient 0.0023 (right)

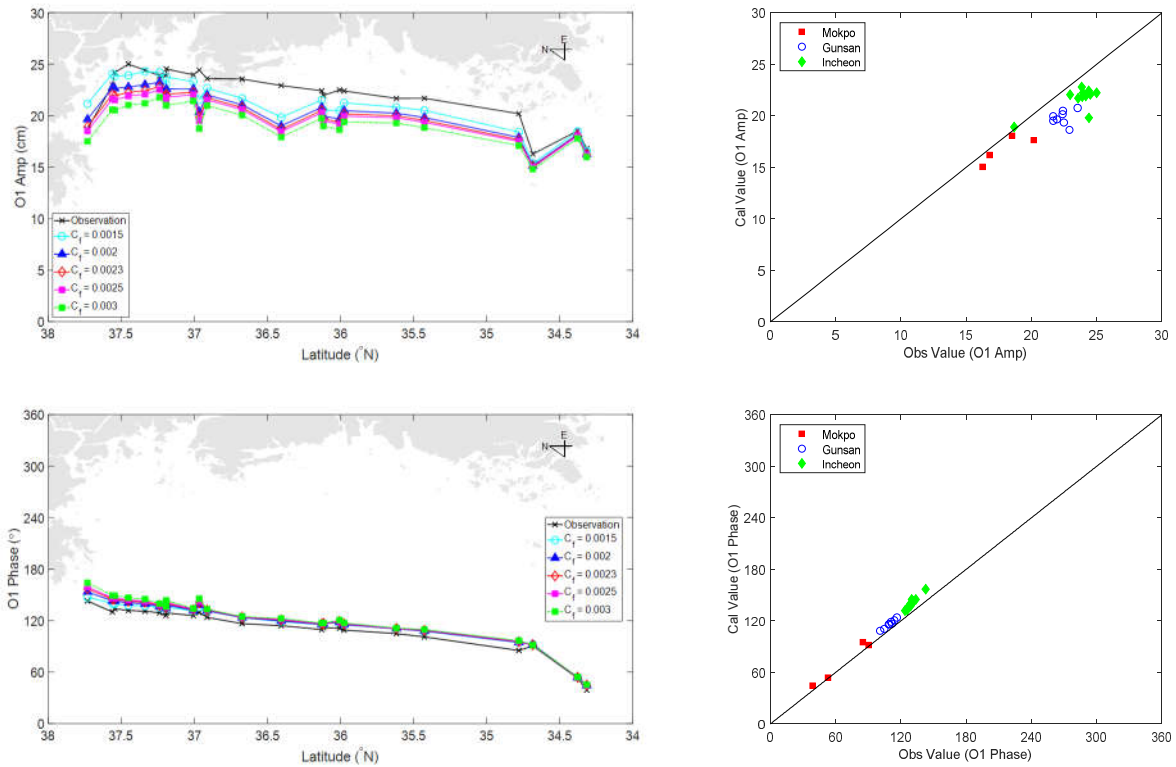

Figure 12. Comparison between the observation data and the computed amplitudes and phase of O1 corresponding to bottom friction coefficient (left) and Comparison between the observation data and the computed amplitudes and phase of O1 with bottom friction coefficient 0.0023 (right)

Table 6. RMSE compared between the observation data and the computed amplitudes (NAO99Jb)

Ocean Tide Model	Tidal Consitituent	C_f	RMSE (cm)			
			Mokpo (M)	Gunsan (G)	Incheon (I)	Mean
NAO99Jb	M2	0.0015	23.07	40.56	45.18	40.51
		0.002	21.69	26.96	19.39	22.68
		0.0023	20.82	19.93	14.16	17.59
		0.0025	20.19	15.75	17.64	17.50
		0.003	19.31	10.46	33.32	25.18
	K1	0.0015	1.22	1.65	2.17	1.86
		0.002	1.10	1.35	2.13	1.73
		0.0023	1.08	1.47	2.42	1.94
		0.0025	1.09	1.64	2.70	2.15
		0.003	1.22	2.30	3.60	2.88
	S2	0.0015	8.78	11.03	12.85	11.61
		0.002	8.39	7.07	19.89	14.79
		0.0023	8.17	6.39	24.02	17.37
		0.0025	7.99	6.77	26.70	19.18
		0.003	7.79	9.32	32.58	23.42
	O1	0.0015	1.12	0.84	1.49	1.24
		0.002	1.01	1.21	1.22	1.18
		0.0023	1.02	1.53	1.46	1.42
		0.0025	1.05	1.75	1.69	1.62
		0.003	1.18	2.28	2.37	2.18

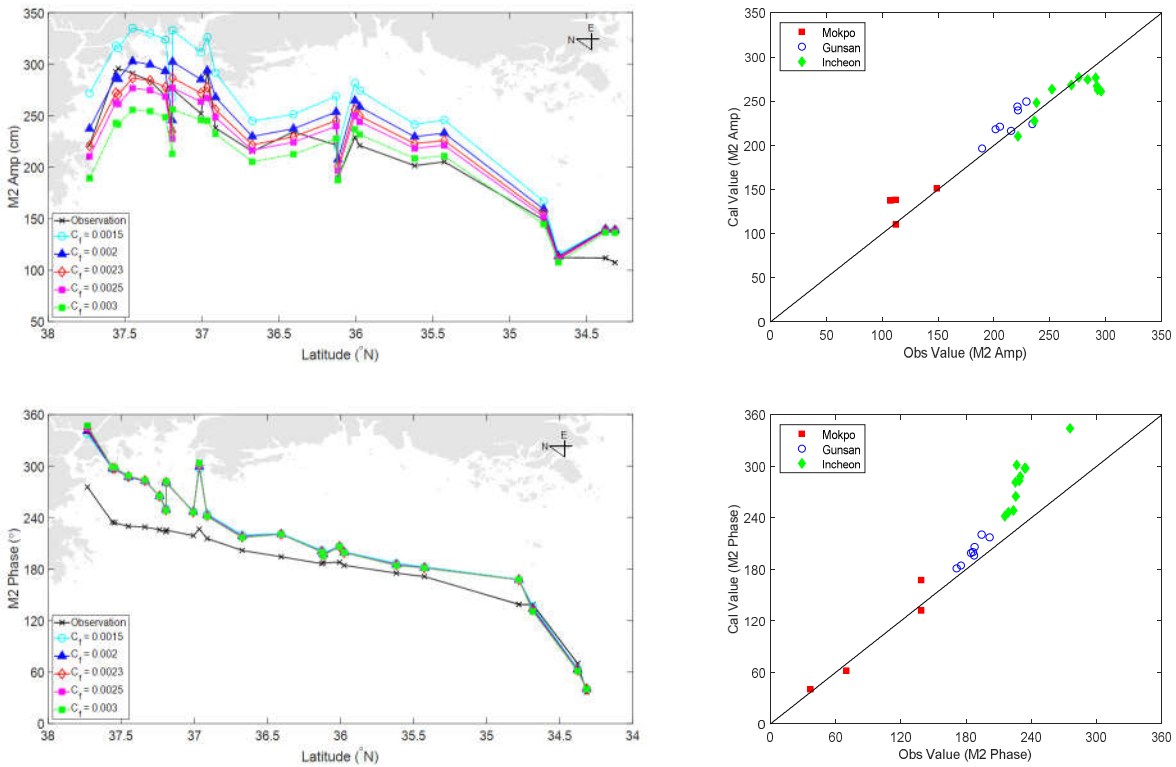

Figure 13. Comparison between the observation data and the computed amplitudes and phase of M2 corresponding to bottom friction coefficient (left) and Comparison between the observation data and the computed amplitudes and phase of M2 with bottom friction coefficient 0.0025 (right)

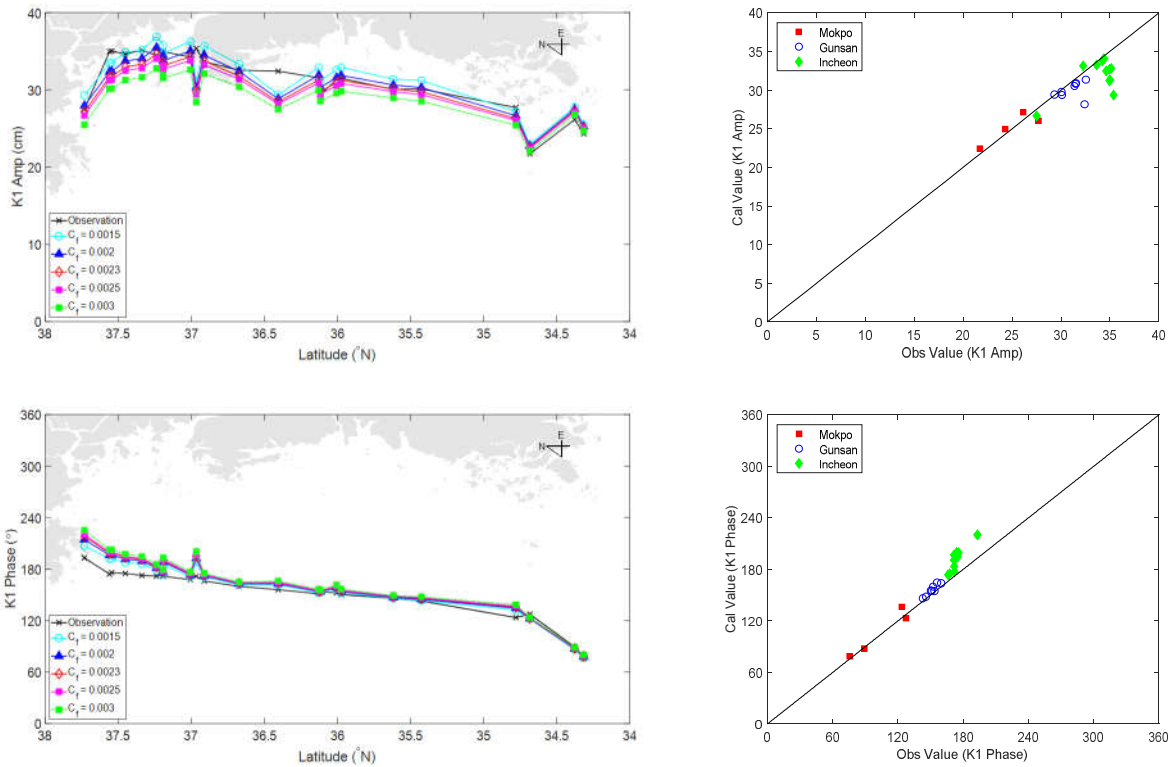

Figure 14. Comparison between the observation data and the computed amplitudes and phase of K1 corresponding to bottom friction coefficient (left) and Comparison between the observation data and the computed amplitudes and phase of K1 with bottom friction coefficient 0.0025 (right)

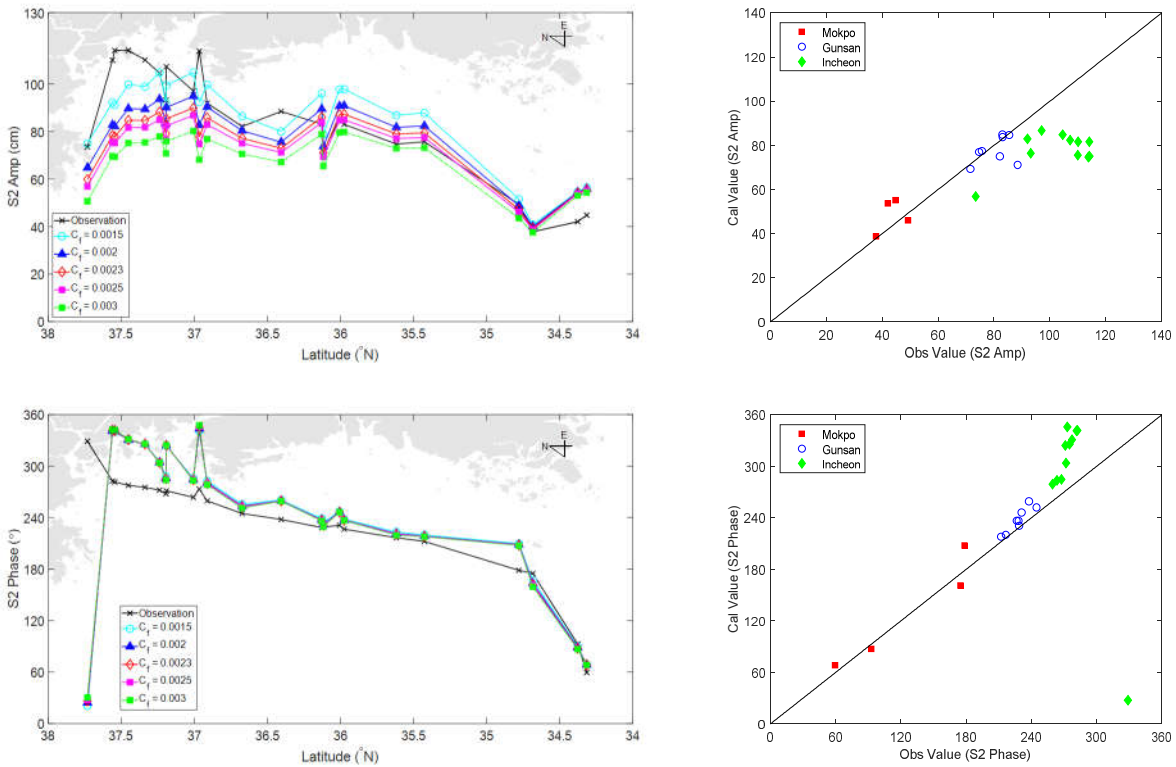

Figure 15. Comparison between the observation data and the computed amplitudes and phase of S2 corresponding to bottom friction coefficient (left) and Comparison between the observation data and the computed amplitudes and phase of S2 with bottom friction coefficient 0.0025 (right)

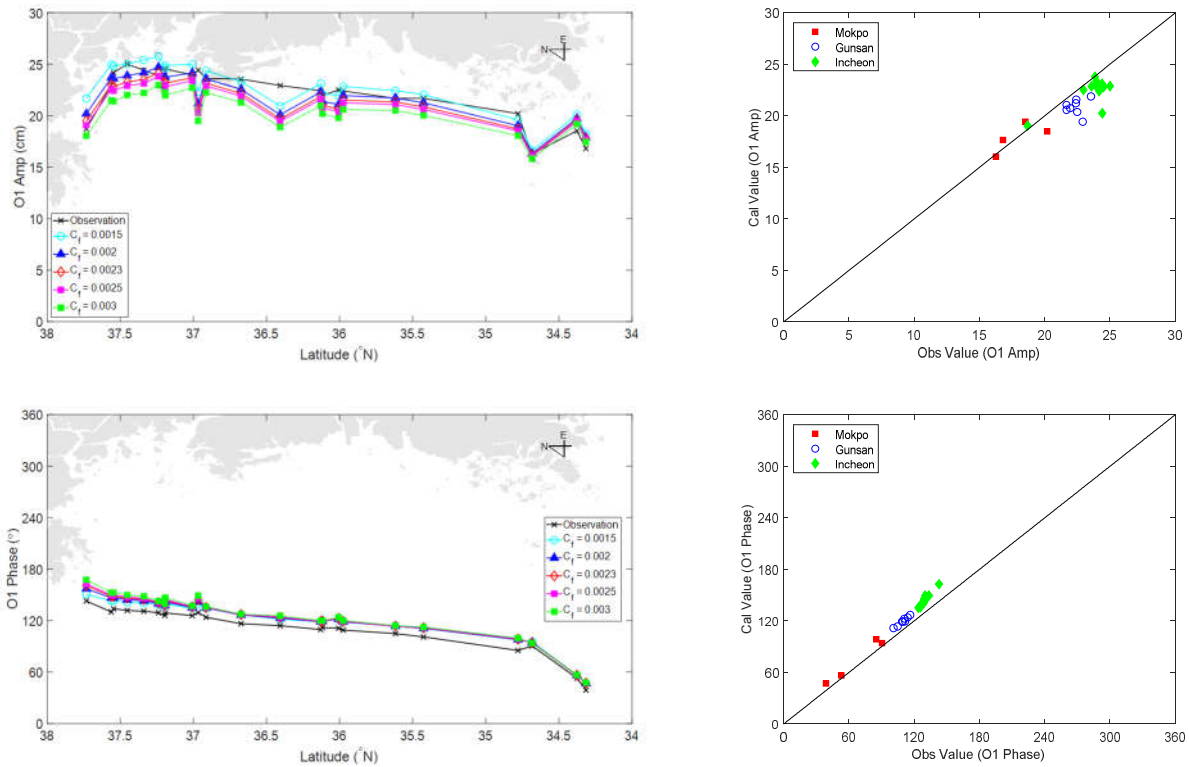

Figure 16. Comparison between the observation data and the computed amplitudes and phase of O1 corresponding to bottom friction coefficient (left) and Comparison between the observation data and the computed amplitudes and phase of O1 with bottom friction coefficient 0.0025 (right)

Table 7. RMSE compared between the observation data and the computed amplitudes (TPXO9.1)

Ocean Tide Model	Tidal Consitituent	C_f	RMSE (cm)			
			Mokpo (M)	Gunsan (G)	Incheon (I)	Mean
TPXO9.1	M2	0.0015	18.54	34.68	40.07	35.30
		0.002	17.12	21.39	15.72	18.12
		0.0023	16.55	15.14	14.63	15.16
		0.0025	16.43	12.13	19.90	16.96
		0.003	15.76	11.13	36.85	27.13
	K1	0.0015	1.55	2.02	2.46	2.17
		0.002	1.33	1.36	1.91	1.64
		0.0023	1.25	1.21	1.93	1.60
		0.0025	1.19	1.25	2.10	1.71
		0.003	1.15	1.75	2.87	2.29
	S2	0.0015	7.74	10.22	12.63	11.09
		0.002	7.36	6.53	19.79	14.54
		0.0023	7.14	6.26	24.07	17.31
		0.0025	7.23	6.76	26.51	19.00
		0.003	6.99	9.54	32.34	23.25
	O1	0.0015	0.81	1.31	1.24	1.20
		0.002	1.04	1.95	1.55	1.63
		0.0023	1.20	2.33	1.98	2.00
		0.0025	1.28	2.50	2.25	2.21
		0.003	1.57	3.09	3.00	2.84

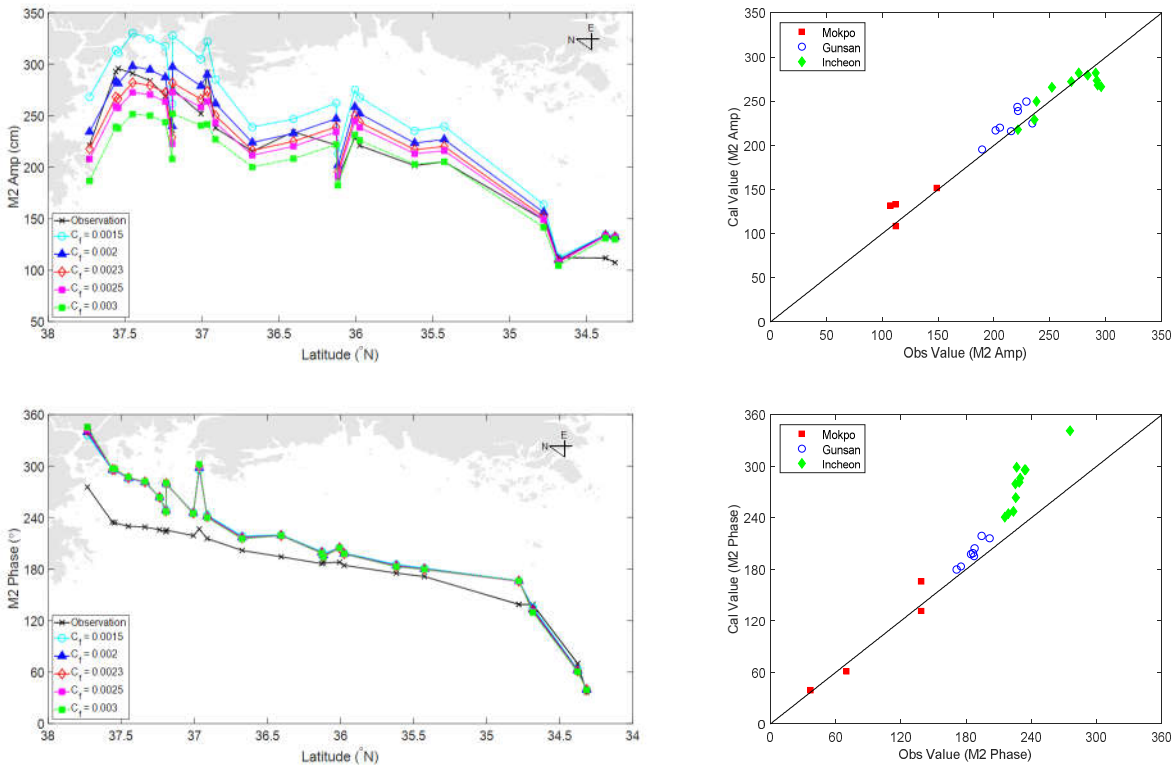

Figure 17. Comparison between the observation data and the computed amplitudes and phase of M2 corresponding to bottom friction coefficient (left) and Comparison between the observation data and the computed amplitudes and phase of M2 with bottom friction coefficient 0.0023 (right)

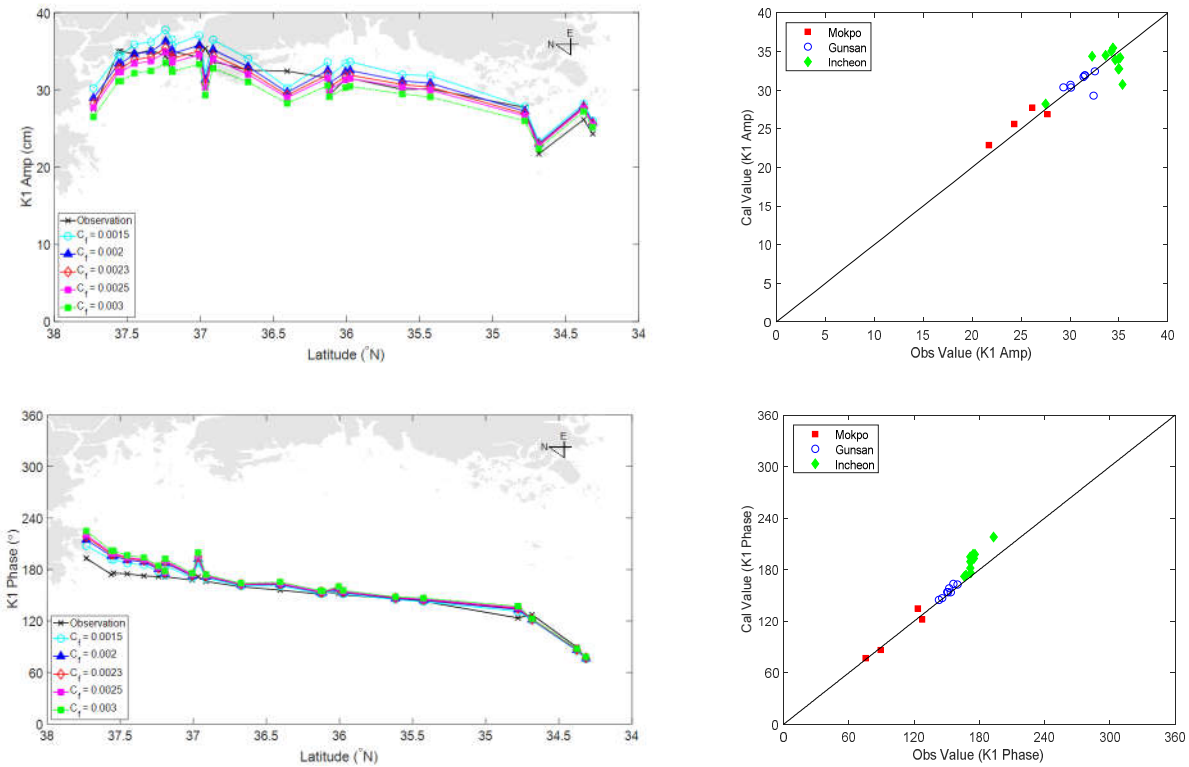

Figure 18. Comparison between the observation data and the computed amplitudes and phase of K1 corresponding to bottom friction coefficient (left) and Comparison between the observation data and the computed amplitudes and phase of K1 with bottom friction coefficient 0.0023 (right)

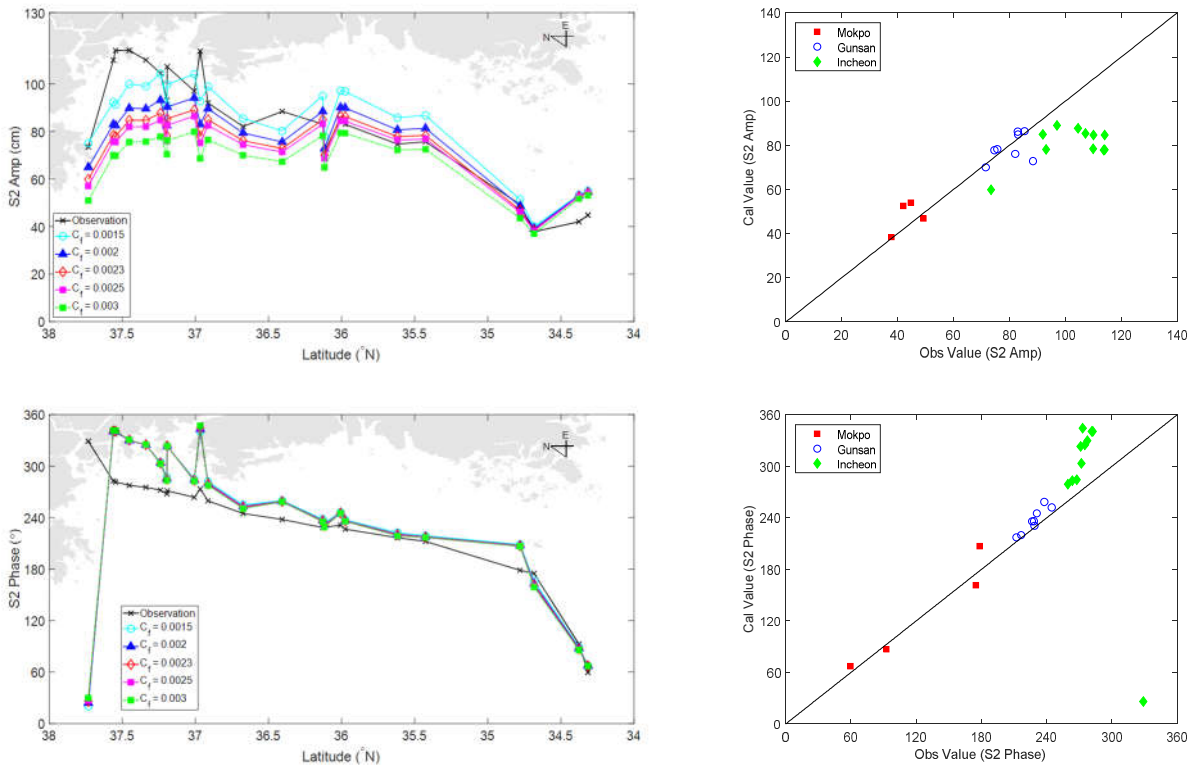

Figure 19. Comparison between the observation data and the computed amplitudes and phase of S2 corresponding to bottom friction coefficient (left) and Comparison between the observation data and the computed amplitudes and phase of S2 with bottom friction coefficient 0.0023 (right)

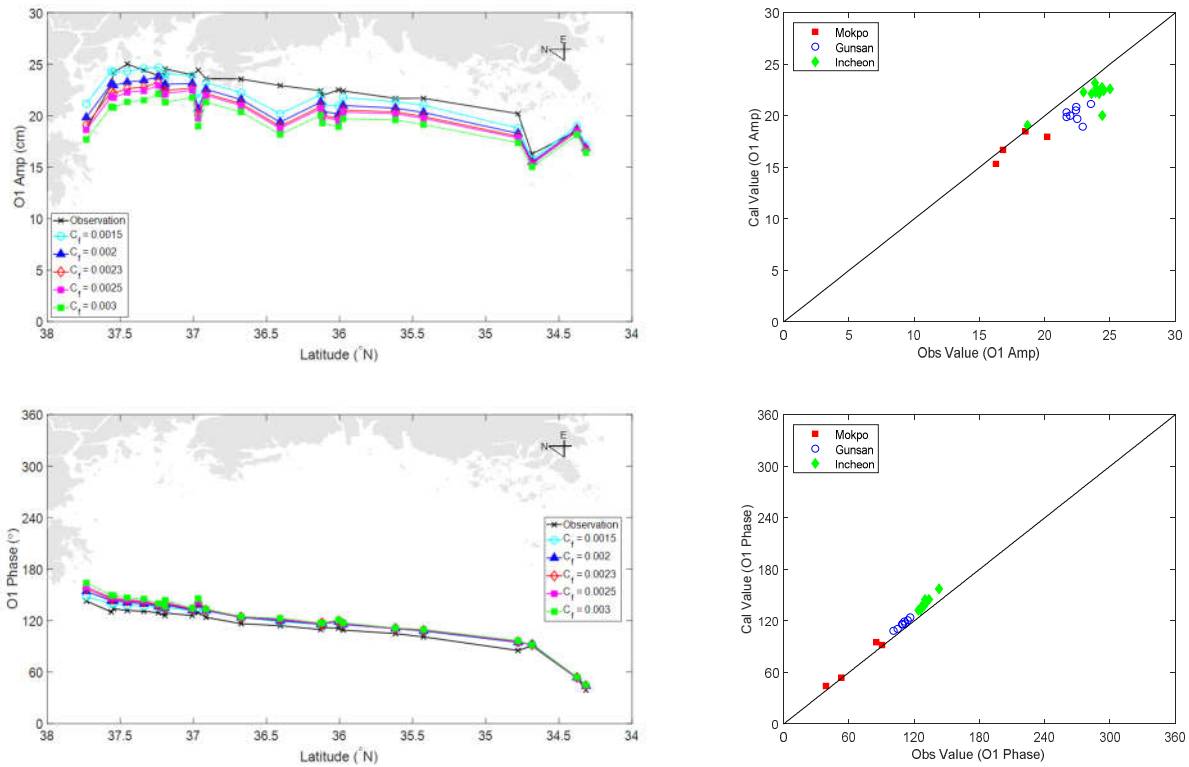

Figure 20. Comparison between the observation data and the computed amplitudes and phase of O1 corresponding to bottom friction coefficient (left) and Comparison between the observation data and the computed amplitudes and phase of O1 with bottom friction coefficient 0.0023 (right)

Table 8. RMSE compared between the observation data and the computed M2 amplitudes with different bottom friction coefficient depending on the regions

Tidal Constituent	Simulation Case	RMSE (cm)			
		Mokpo (M)	Gunsan (G)	Incheon (I)	Mean
M2	FES 2-1	17.57	12.04	11.94	13.13
	FES 2-2	17.58	11.77	11.90	13.02
	FES 2-3	17.86	11.61	12.12	13.14
	FES 2-4	17.06	11.40	12.06	12.86
	NAO 2-1	20.42	15.00	12.75	15.12
	NAO 2-2	20.29	14.15	12.38	14.65
	NAO 2-3	20.31	13.39	13.83	15.02
	NAO 2-4	20.28	13.53	12.03	14.30
	TPX 2-1	15.95	11.09	11.91	12.45
	TPX 2-2	16.40	11.17	11.91	12.57
	TPX 2-3	16.24	11.24	12.09	12.64
	TPX 2-4	16.49	11.18	11.68	12.49

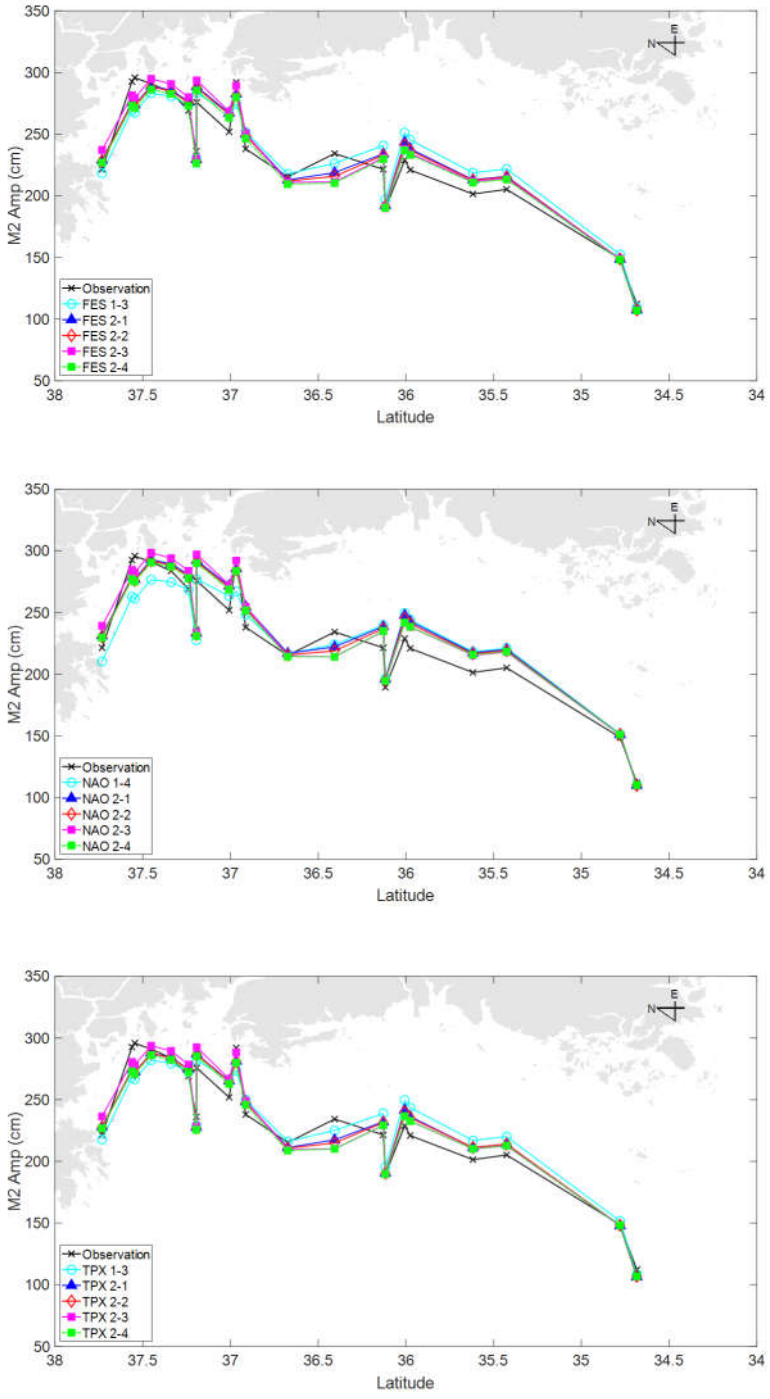

Figure 21. Comparison between the observation data and the computed M2 amplitudes with different bottom friction coefficient depending on the regions

4.2 Type of Tide

It is noted that the over-tide and compound tide are produced when tidal flow approaches coastal area. These types of tides cannot change the type of tides, but it can change the shape of tides because the types of tides merge into another, for example, M2 and S2 can produce M4 and MS4.

Below criterion is introduced that which type of tide is considered in that region.

$$(K_1 + O_1) / (M_2 + S_2)$$

If the ratio of the amplitudes in accordance with the above criterion is less than 0.25, the tide is considered semi-diurnal. If the ratio is between 0.25 and 1.25, it is mixed tide, and if it is more than 1.25, it is diurnal tide.

Semi-diurnal tides were mostly dominant around the West Coast of Korea in accordance with observation data and numerical results. Therefore, it was important to obtain accurate data for semi-diurnal tide such as M2 and S2.

Table 9. Criterion values for the type of tide at the tide stations

Station No.	Observation	FES 1-3	NAO 1-4	TPX 1-3
M1	0.27	0.22	0.22	0.23
M2	0.29	0.24	0.24	0.25
M3	0.25	0.25	0.26	0.26
M4	0.24	0.22	0.23	0.23
G1	0.18	0.16	0.17	0.17
G2	0.19	0.17	0.17	0.17
G3	0.18	0.15	0.16	0.16
G4	0.17	0.15	0.15	0.15
G5	0.20	0.18	0.19	0.19
G6	0.18	0.16	0.16	0.16
G7	0.17	0.16	0.16	0.16
G8	0.19	0.18	0.18	0.18
I1	0.17	0.16	0.17	0.17
I2	0.15	0.14	0.15	0.14
I3	0.17	0.16	0.16	0.16
I4	0.16	0.15	0.15	0.15
I5	0.17	0.18	0.18	0.18
I6	0.16	0.16	0.16	0.16
I7	0.15	0.15	0.16	0.16
I8	0.15	0.15	0.15	0.15
I9	0.14	0.16	0.16	0.16
I10	0.14	0.15	0.16	0.16
I11	0.16	0.17	0.17	0.17

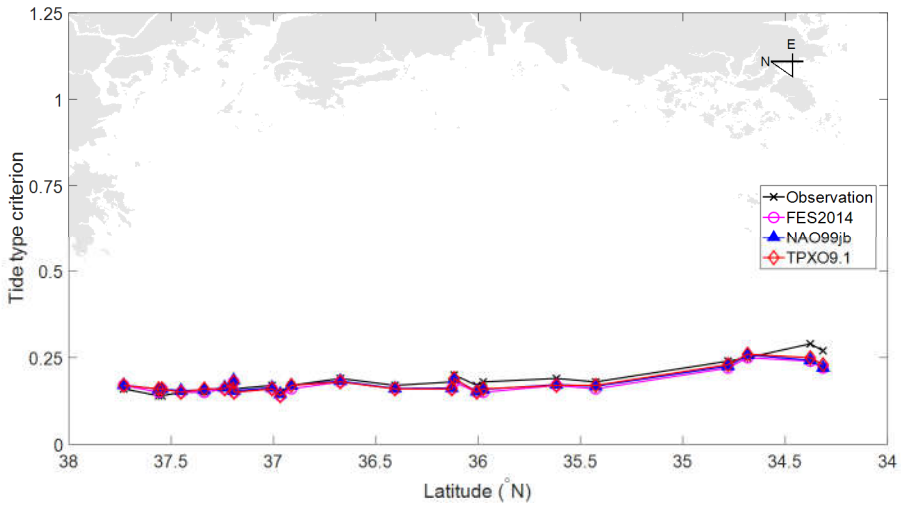

Figure 22. Comparison graph for the criterion values at the tide stations

CHAPTER 5. SENSITIVITY ANALYSIS

5.1 Response to Individual Boundary Forcing

Sensitivity analyses were carried out to find out three individual open boundary effect on the tidal elevation along the West Coast of Korea.

Firstly, the amplitude of M2 or K1 with 100 cm was imposed on each open boundary individually. M2 and K1 are the most dominant tidal constituents in semi-diurnal tides and diurnal tides among the tidal constituents. The numerical results of amplitude at the tide stations for assumed tidal forcing to each open boundary were shown in Figure 23 and Figure 24. From that results, it was noticed that the tide was amplified along the West Coast of Korea by the flow from the open boundary B in case of both M2 and K1. Trend of tide amplification was similar to the observation data when imposing the tidal amplitude on the open boundary B. The tide was not amplified when the tidal amplitude was forced on the open boundary A or C. Thus, the tidal flow from the open boundary B played an important role in tidal elevation along the West Coast of Korea.

Second, the amplitude of M2 in the boundary condition data used in the fourth section was increased by 10 cm for each open boundary respectively and these modified open boundary conditions were used for the sensitivity analysis. Sequential sensitivity analyses were carried out for K1 tidal constituent. Numerical results were compared with the results in the previous chapter in

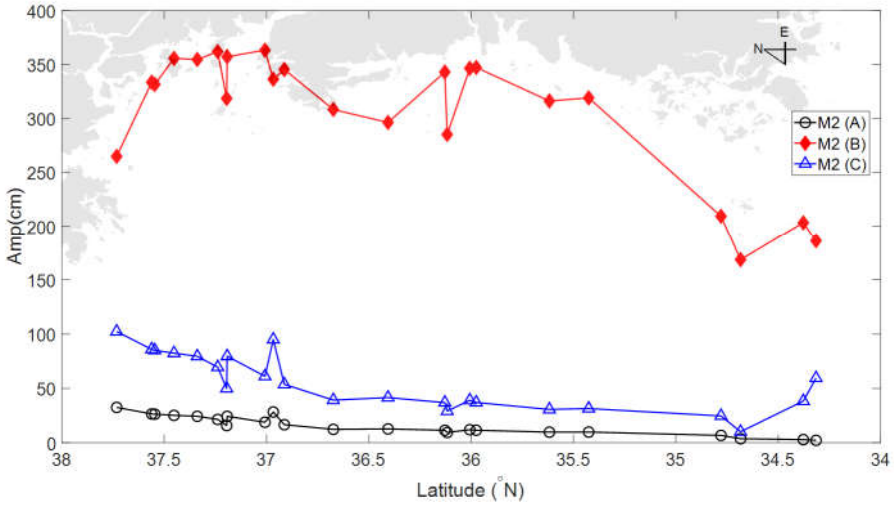

Figure 23. Computed amplitudes with respect to the assumed forcing with the amplitude 100cm of M2 at each open boundary, A, B, and C

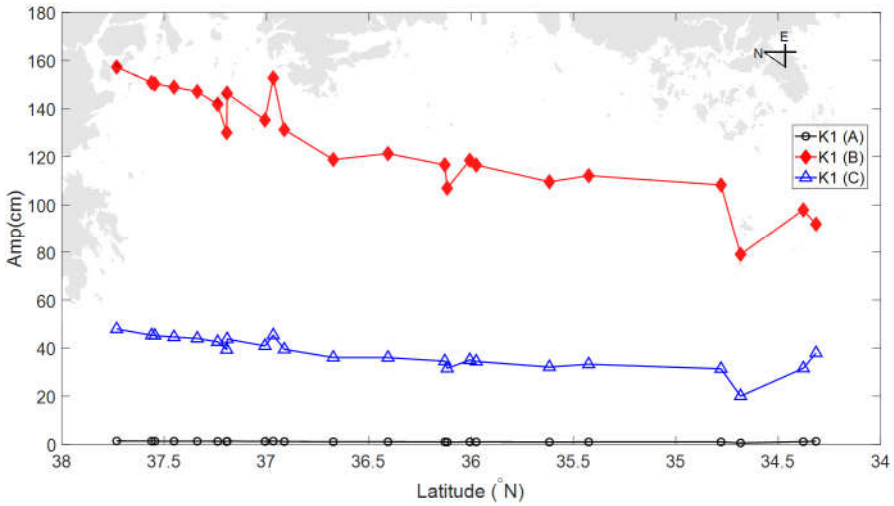

Figure 24. Computed amplitudes with respect to the assumed forcing with the amplitude 100cm of K1 at each open boundary, A, B, and C

order to see how much the tide change depend on changing of the open boundary conditions. This method was used in Choi (1980). The base model for these sensitivity tests was FES 1-3. The results showed the same tendency as the sensitivity analysis in previous. The tidal flow from the open boundary B mostly affected to the tidal elevation around the West Coast of Korea rather than boundary A and C. Differences in amplitude between the FES 1-3 and the newly established models were shown in Table 10 and Table 11.

Table 10. Differences in the amplitude of M2

Station No.	M2-A	M2-B	M2-C
M1	0.07	-19.68	-5.54
M2	0.00	-21.09	-4.00
M3	-0.15	-16.37	-1.65
M4	-0.15	-15.83	-1.80
G1	-0.31	-28.39	-2.79
G2	-0.31	-28.48	-2.77
G3	-0.35	-30.12	-2.94
G4	-0.36	-28.51	-2.80
G5	-0.28	-25.82	-2.51
G6	-0.34	-30.12	-2.93
G7	-0.27	-21.69	-2.21
G8	-0.29	-26.81	-2.62
I1	-0.32	-28.10	-2.78
I2	-0.23	-18.86	-2.00
I3	-0.33	-28.71	-2.86
I4	-0.28	-22.90	-2.37
I5	-0.29	-26.32	-2.61
I6	-0.31	-26.65	-2.70
I7	-0.28	-22.86	-2.38
I8	-0.27	-22.36	-2.31
I9	-0.25	-19.81	-2.10
I10	-0.25	-19.81	-2.11
I11	-0.18	-13.83	-1.46

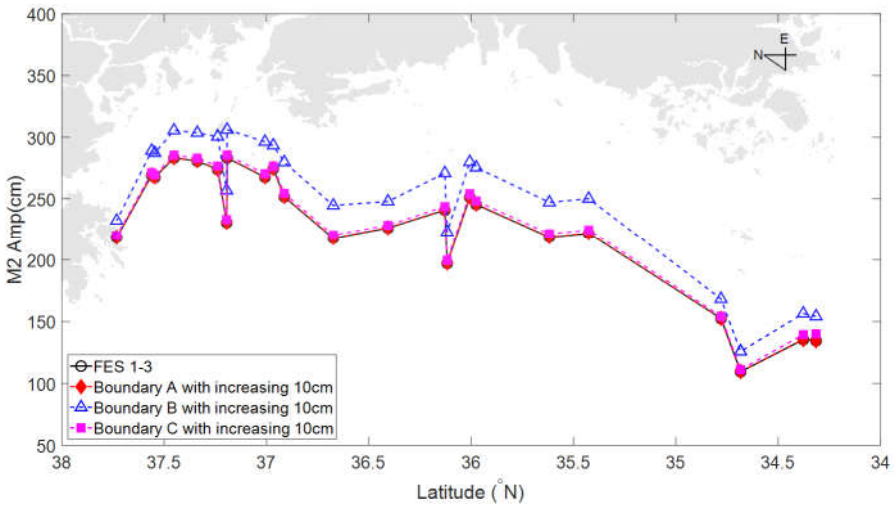

Figure 25. Comparison between FES 1-3 and computed M2 amplitudes

Table 11. Differences in the amplitude of K1

Station No.	K1-A	K1-B	K1-C
M1	-0.02	-10.05	0.36
M2	0.00	-11.06	0.61
M3	0.01	-9.57	0.69
M4	0.00	-11.08	0.79
G1	0.00	-12.65	0.99
G2	0.01	-12.71	1.00
G3	0.00	-13.37	1.05
G4	-0.01	-13.48	1.04
G5	0.01	-12.61	0.99
G6	0.01	-13.30	1.05
G7	0.02	-12.06	0.93
G8	0.02	-13.47	1.07
I1	0.01	-14.38	1.15
I2	0.03	-12.83	1.06
I3	0.01	-14.51	1.17
I4	0.02	-13.97	1.15
I5	0.02	-14.28	1.14
I6	0.02	-14.57	1.19
I7	0.02	-13.98	1.16
I8	0.02	-13.99	1.15
I9	0.03	-13.59	1.14
I10	0.01	-13.64	1.16
I11	0.03	-12.33	1.02

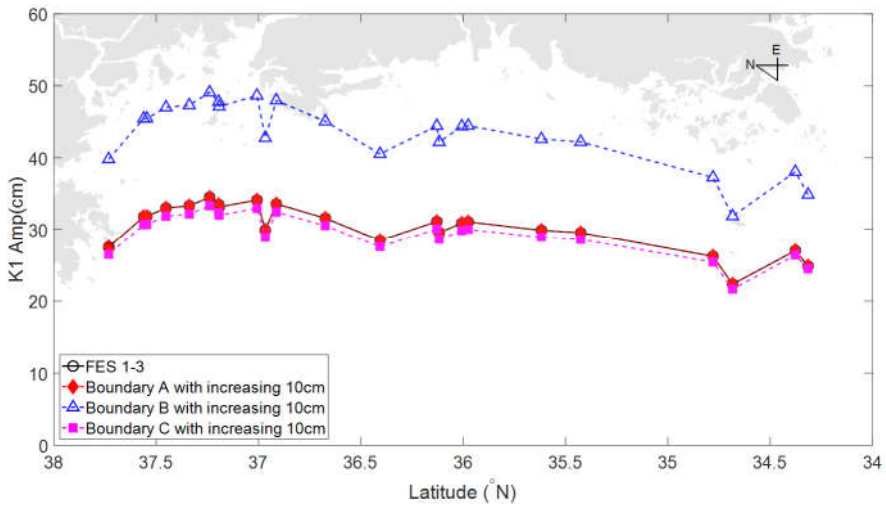

Figure 26. Comparison between FES 1-3 and computed K1 amplitudes

5.2 Response to the Tidal Amplitude at the Open Boundary

From the sensitivity analyses done in section 5.1, it was noticed that tidal forcing from open boundary B highly affected tidal elevation along the West Coast of Korea. In this section, quantitative assessment of the influence of boundary tide amplitudes to the tidal elevation along the West Coast of Korea. Mean increase of amplitude (D_a) on each tide station with respect to the variation of boundary amplitude was calculated by the following equation.

$$D_{a,j} = \frac{r_i(a_2) - r_i(a_1)}{a_2 - a_1}$$

where

a_1, a_2 : different tidal amplitude on boundary B

Different amplitudes, 20cm, 40cm, 60cm, 80cm, and 100cm, of M2 or K1, were forced on the open boundary B. The amplitudes of M2 and K1 with the given boundary amplitude at the tide stations were shown in Figure 27 and Figure 28. The mean increase values in the classified regions were indicated in Table 12 and Table 13. In the case of M2, the mean increase values decreased as the interval of the boundary amplitude became higher. On the other hand, the mean increase values for K1 increased as the interval of the boundary amplitude became higher. The mean increase values for M2 were lager than the values for K1. As described in the variation of M2 and K1 with the change of boundary forcing at the open boundary, the amplitude of M2 was more sensitively changed than the amplitude of K1.

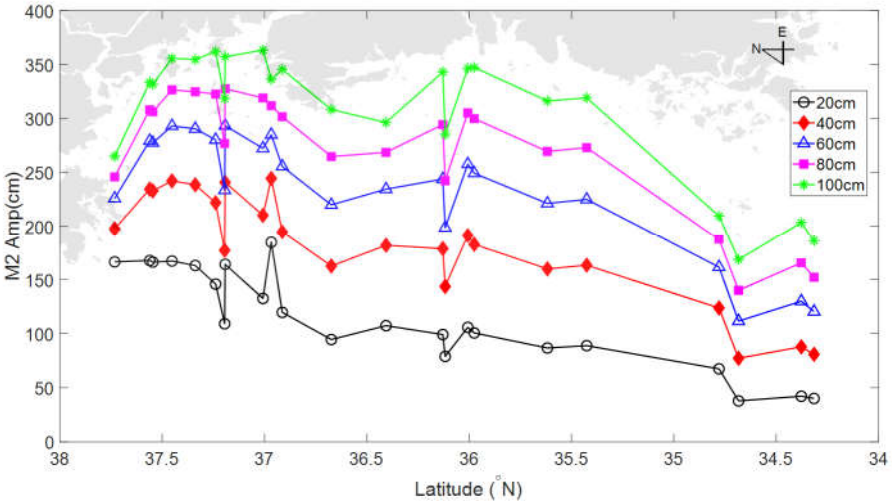

Figure 27. M2 amplitudes at the tide stations with respect to the boundary forcing with the amplitudes of 20 cm, 40 cm, 60 cm, 80 cm, and 100 cm at the open boundary B

Table 12. D_a per 1cm increase of the tidal amplitude of M2 on the open boundary B

Tidal Constituent	$a_1 - a_2$	D_a			
		Incheon	Gunsan	Mokpo	Mean
M2	20-40	3.40	3.76	2.28	2.57
	40-60	2.51	3.04	1.92	2.15
	60-80	1.75	2.30	1.52	1.70
	80-100	1.60	2.15	1.53	1.68

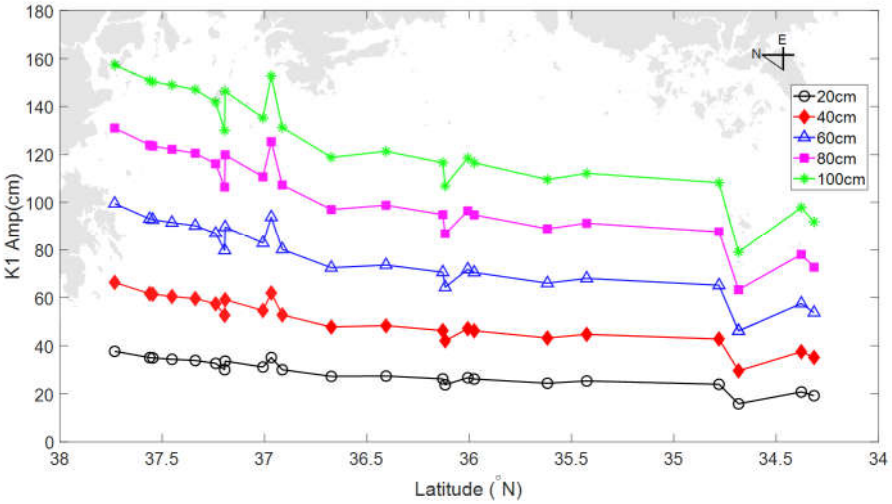

Figure 28. K1 amplitudes at the tide stations with respect to the boundary forcing with the amplitudes of 20 cm, 40 cm, 60 cm, 80 cm, and 100 cm at the open boundary B

Table 13. D_a per 1cm increase of the tidal amplitude of K1 on the open boundary B

Tidal Constituent	$a_1 - a_2$	D_a			
		Incheon	Gunsan	Mokpo	Mean
K1	20-40	1.27	0.99	0.81	0.85
	40-60	1.51	1.20	0.97	1.01
	60-80	1.48	1.20	0.99	1.02
	80-100	1.30	1.07	0.94	0.96

In all cases, the maximum amplitude of M2 and K1 occurred in Incheon region. Mokpo region has lots of islands, and water depth changes rapidly in Mokpo region and Gunsan region. On the other hand, change in water depth is relatively moderate in Incheon region rather than Mokpo region and Gunsan region. Therefore, the energy is less dissipated in Incheon region than other regions. It can be explained why the tidal elevation in Incheon region was larger than other regions. The mean increase of amplitude were computed from the numerical models with the amplitude of M2 or K1 tidal constituent from the open boundary condition data used in the fourth section which were increased by 10cm, 20cm, and 30cm for the open boundary B respectively. The results were presented in Figure 29, Figure 30, Table 14, and Table 15. The tendency of the values of mean increase of amplitude was similar to the results from the model with uniform amplitude on the open boundary B. From that results, it was noticed that the M2 amplitude sensitively responds to open boundary conditions rather than K1 amplitude.

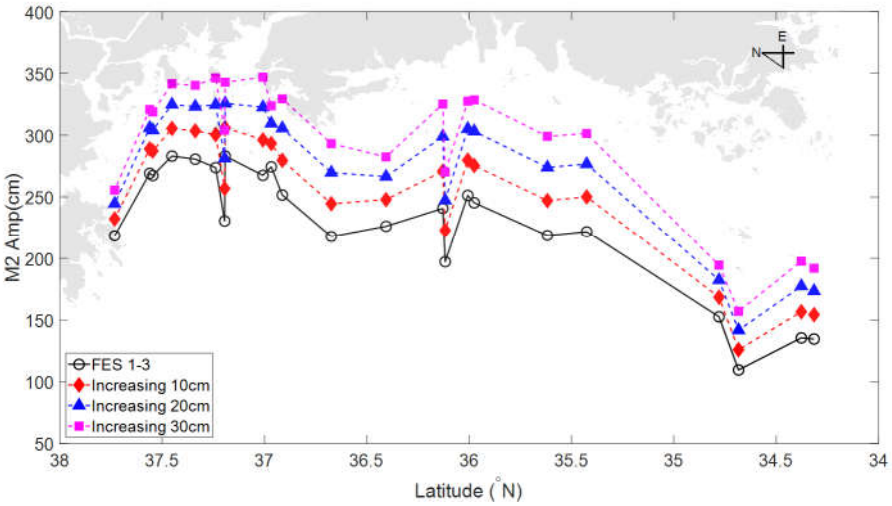

Figure 29. M2 amplitude at the tide stations with respect to the forcing with increasing amplitudes at the open boundary B

Table 14. D_a per 1cm increase of the tidal amplitude of M2 with respect to increasing amplitude on the open boundary B

Tidal Constituent	$a_1 - a_2$	D_a			
		Incheon	Gunsan	Mokpo	Mean
M2	10-20	2.02	2.54	1.74	2.15
	20-30	1.80	2.33	1.65	1.96

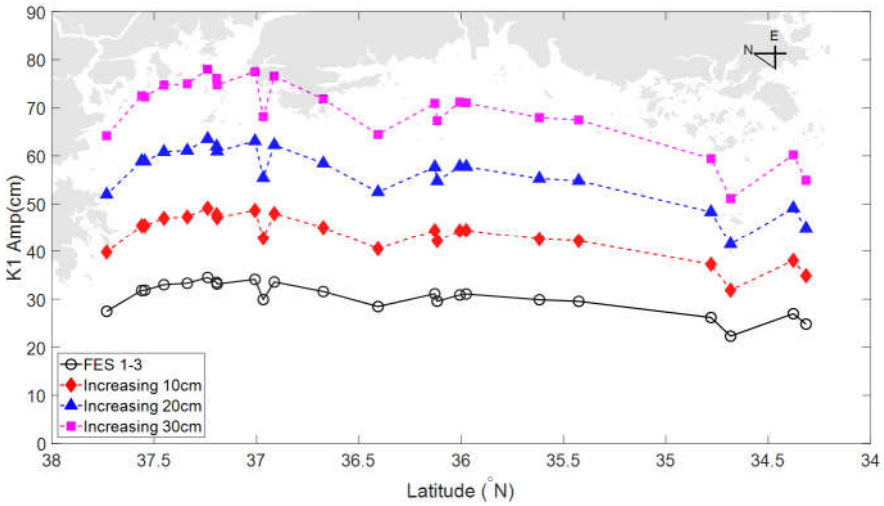

Figure 30. K1 amplitude at the tide stations with respect to the forcing with increasing amplitudes at the open boundary B

Table 15. D_a per 1cm increase of the tidal amplitude of K1 with respect to increasing amplitude on the open boundary B

Tidal Constituent	$a_1 - a_2$	D_a			
		Incheon	Gunsan	Mokpo	Mean
K1	10-20	1.37	1.29	1.04	1.28
	20-30	1.37	1.29	1.05	1.29

The nonlinear response of tidal amplitude along the West Coast of Korea was evaluated by the following sensitivity estimation.

$$R_{a,i} = \frac{r_i(a_2) / r_i(a_1)}{a_2 / a_1}$$

where

$r_i(a_1)$: amplitude at i-th tide station with boundary amplitude a_1

$r_i(a_2)$: amplitude at i-th tide station with boundary amplitude a_2

a : imposed uniform boudary amplitude

The $r(a)$ was defined to be the tidal amplitude at the tide stations generated by applying the tidal forcing with amplitude a to the open boundary B. The value of a_1 was fixed to be 20 cm and $R_{a,i}$ was calculated at each tide station by imposing the boundary amplitude a_2 of M2 or K1 with 40 cm, 60 cm, 80 cm, and 100 cm. If the amplitudes change linearly corresponding to changing the open boundary amplitude, the value of $R_{a,i}$ is about 1. However, the $R_{a,i}$ values were not 1 both M2 and K1. When the tide was going from Mokpo to Incheon, the $R_{a,i}$ values were farther from 1. That meant that the increasing of the tidal amplitude was started to depress when the tide propagated along the coastlines.

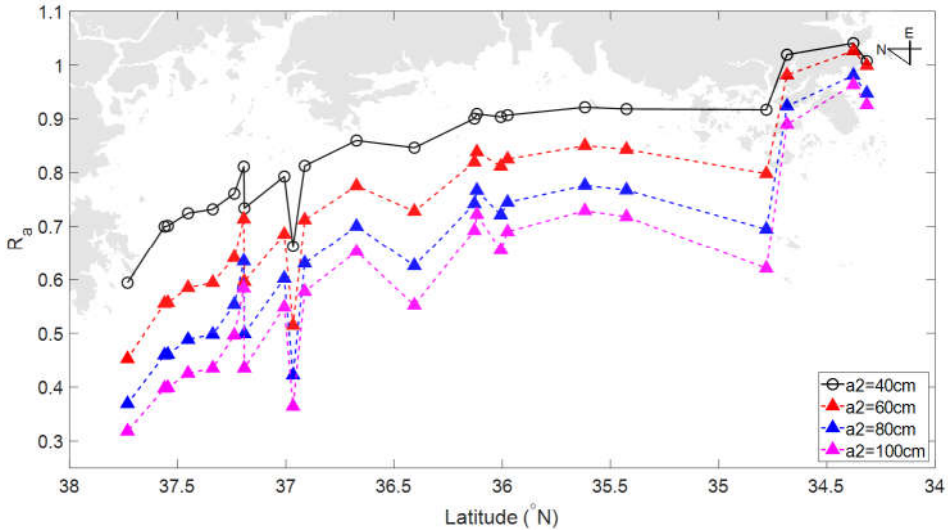

Figure 31. Nonlinear response at tide station for M2 with respect to the increase of amplitude at the open boundary B

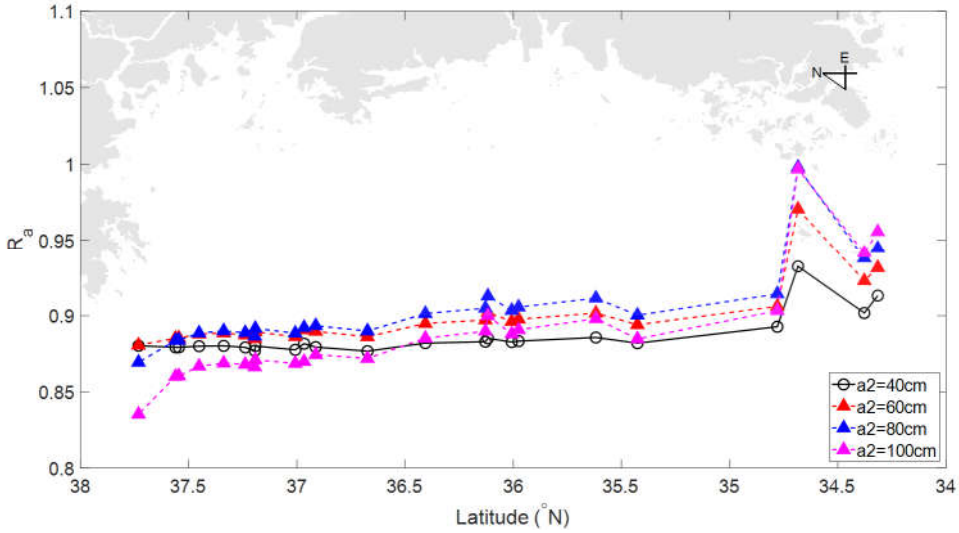

Figure 32. Nonlinear response at tide station for K1 with respect to the increase of amplitude at the open boundary B

CHAPTER 6. CONCLUSION

Tidal models were constructed using Telemac-2D in order to reproduce tidal elevation around the West Coast of Korea. The main objective was that the effect of bottom roughness and open boundary conditions on tidal elevation around the West Coast of Korea was examined.

For that purpose, five different values of bottom friction coefficient were uniformly applied to the numerical model, respectively and then three different values of bottom friction coefficient depending on the regions were applied to the models. Three well-known tide models, FES2014, NAO99Jb, and TPXO9.1, were used to set open boundary conditions. The numerical results were evaluated by dividing three regions, Mokpo, Gunsan, and Incheon. Sensitivity analyses were carried out to find out characteristics of the tidal elevation around the West Coast of Korea.

Tidal elevation near the coastline was sensitively varied by bottom friction coefficient, especially amplitude of M2 and S2 rather than that of K1 and O1. In addition, different bottom friction coefficients were required depending on the regions due to geographic characteristic and bottom roughness. More dissipation of tidal energy occurred in Mokpo region and Gunsan region than Incheon region because the water depth is changed more rapidly in Mokpo region and Gunsan region than Incheon region and there are lots of islands around Mokpo region. Thus, Gunsan region and Mokpo region were required the larger value of bottom friction coefficient rather than Incheon region. When

different values of bottom friction coefficients depending on the regions, the results were in good agreement with observation data, especially M2 tidal constituent rather than the results from the model with uniform bottom friction coefficient. Therefore, it was the way that applying different bottom friction coefficients depending on the regions to get more accurate tide data.

From the sensitivity analyses, the characteristics of the tide around the West Coast of Korea were found out. First, the tidal flow from Okinawa Through had a much greater effect on tidal elevation around the West Coast of Korea than the tidal flow from Taiwan Strait and Korea Strait. Second, the tidal elevation of M2 was more sensitively responded by changing the boundary condition than the tidal elevation of K1. Third, the tidal amplitude changed nonlinearly along the coast even the open boundary conditions on the seaward side changed linearly and the increasing of amplitude was started to depress when the tides propagated along the coastlines.

REFERENCES

An, H.S., 1977. A numerical experiment of the M2 tide in the Yellow Sea. Journal of the Oceanographical Society of Japan, 33 (1977), 103-110.

Arbic, B.K., Scott R.B., 2007. On quadratic bottom drag, geostrophic turbulence, and oceanic mesoscale eddies. Journal of Physical Oceanography 38, 84-103.

Bao, X.W., Gao, G.P., Yan, J., 2000. Three-dimensional simulation of tide and tidal current characteristics in the East China Sea. Oceanologica Acta, 24 (2001), 135-149.

Carrère, L., et al., 2012. FES 2012: A new global tidal model taking advantage of nearly 20 years of altimetry. paper presented at The Symposium 20 Years of Progress in Radar Altimetry, Venice.

Choi, B.H., 1980. A tidal model of the Yellow Sea and the Eastern China Sea. Korean Ocean Research and Development Institute Report 20-02.

Davies, A.M., 1986. A three-dimensional model of the Northwest European Continental Shelf, with application to the M4 tide. Journal of Physical Oceanography, 16 (1986), 797-813.

Davies, A.M., Kwong, S.C.M., Flather R.A., 1997. Formulation of a variable-function three-dimensional model, with applications to the M2 and M4 tide on the North-West European Continental Shelf. Continental Shelf Research, 17 (1997), No. 2, 165-204.

Dronkers, J.J. (1964). Tidal computations.

Egbert, G.D., Erofeeva, S.Y., 2002. Efficient inverse modeling of barotropic ocean tides. Journal of Atmospheric and Oceanic Technology, 19 (2002), 183-204.

Foreman, M.G.G. (1996). Manual for tidal current analysis and prediction.

Foreman, M.G.G., Henry, R.F., 1989. The harmonic analysis of tidal model time series. Advanced Water Resource, 12 (1989), 109-120.

Foreman, M.G.G. (1996). Manual for tidal height analysis and prediction.

Guo, X., Yanagi, T., 1998. Three dimensional structure of tidal current in the East China Sea and the Yellow Sea. Journal of Oceanography 54 (1998), 651-668.

Hervouet, J.M. (2007). Hydrodynamics of free surface flows.

Jones, J.E., Davies, A.M., 2005. An intercomparison between finite difference

and finite element (TELEMAC) approaches to modelling west coast of Britain tides. Ocean Dynamics 55 (2005), 178-198.

Kang, S.K., Lee, S.R., Lie, H.J., 1997. Fine grid tidal modeling of the Yellow and east China seas. Continental Shelf Research 18 (1998), 739-772.

Larsen, L.H., Cannon, G.A., Choi, B.H., 1985. East China Sea tide currents. Continental Shelf Research, 4 (1985), 77-103.

Lee, H.J., Jung, K.T., So, J.K., Chung, J.Y., 2002. A three dimensional mixed finite-difference Galerkin function model for the oceanic circulation in the Yellow Sea and the East China Sea in the presence of M2 tide. Continental Shelf Research 22 (2002), 67-91.

Lee, J.C., Jung, K.T., 1999. Application of eddy viscosity closure models for the M2 tide and tidal currents in the Yellow Sea and the East China Sea. Continental Shelf Research, 19 (1999), 445-475.

Lee, S., Lie, H.J., Cho, C.H., Kang, S.K., Teague, W.J., Chang, K.I., Song, K.M., Oh, K.H. 2011. Vertical structure of the M2 tidal current in the Yellow Sea. Ocean Science Journal, (2011) 46(2), 73-84.

Lefevre, F., Provost, C.L., Lyard, F.H., 2000. How can we improve a global ocean tide model at a regional scale? A test on the Yellow Sea and the East China Sea. Journal of Geophysical Research, 105, No. C4, 8707-8725.

Lu, X., Zhang, J. 2006. Numerical study on spatially varying bottom friction coefficient of a 2D tidal model with adjoint method. Continental Shelf Research, 26 (2006), 1905-1923.

Liu, Q., Wang, D., Lv, X., 2014. A study on bottom friction coefficient in the Bohai, Yellow, and East China Sea. Mathematical Problems in Engineering, Vol 2014, 7.

Matsumoto, K., Takanezwa, T., Ooe, M., 2000. Ocean tide models developed by assimilating TOPEX/POEIDON altimeter data into hydrodynamical Model: a global model and regional model around Japn. Journal of Oceanography, 56 (2000), 567-581.

Naimie, C.E., Blain, C.A., Lynch, D.R., 2001. Seasonal mean circulation in the Yellow Sea – a model generated climatology. Continental Shelf Research, 21 (2001), 667-695.

Niwa Y., Hibiya, T., 2004. Three-dimensional numerical simulation of M2 internal tides in the East China Sea. Journal of Geophysical Research, 109, C04027.

Pawlowicz R., Beardsley B., Lentz S., 2002. Classical tidal harmonic analysis

including error estimates in MATLAB using T_TIDE. Coputers and Geosciences 28 (2002) 929-937.

Pingree, R.D., Griffiths, D.K., 1987. Tidal friction for semidiurnal tides. Continental Shelf Research, 7 (10), 1181-1209.

Prandle, D., 1997. The influence of bed friction and vertical eddy viscosity on tidal propagation. Continental Shelf Research, 17 (11), 1367-1374.

Sauvaget, P., David, E., Soares, C.G., 2000. Modelling tidal currents on the coast of Portugal. Coastal Engineering 40 (2000), 393-409.

Suh, S.W., 2011. Reproduction of shallow tides and tidal asymmetry by using finely resolved grid on the West Coast of Korea. Journal of Korean Society of Coastal and Ocean Engineering 23 (4), 313-325.

Teague, W.J., Perkins, H.T., Hallock, Z.R., Jacobs, G.A., 1998. Current and tide observations in the southern Yellow Sea. Journal of Geophysical Research, 103 (1998), 27,783-27,793.

Westerink, J.J., Luettich R.A., Muccino, J.C., 1994. Modeling tides in the western North Atlantic using unstructured grids. Tellus (1994) 46A, 178-199.

Xia, C.S., Qiao, F.G., Yang, Y.Z., Ma, J., Yuan, Y., 2006. Three dimensional structure of the summertime circulation in the Yellow Sea from a wave-tide-circulation coupled model. Journal of Geophysical Research, 111, C11S03.

Yanagi, T. and Inoue, K., 1994. Tide and tidal current in the Yellow/East China Seas. La mer 32 (1994), 153-165.

Zhao, B., Fang, G.H., Cao, D., Numerical modeling on the tides and tidal currents in the Eastern China Seas. Yellow Sea Research 5 (1993), 41-61.

Zu, T., Gan, J.P., Erofeeva, S.Y. 2008. Numerical study of the tide and tidal dynamics in the south China sea. Deep-Sea Research 1 55 (2008), 137-154.

초록

한국 서해안에서의 조석은 그 크기가 크며, 조류 또한 빠르고 조석에 민감하게 변화하는 특성을 가지고 있다. 게다가 조석은 서해안의 해수 흐름의 주 요인이기 때문에 조석에 대한 정확한 예측과 그 특징의 이해가 필요하다.

본 연구에서는 조도계수와 개방경계조건이 서해안의 조석에 미치는 영향을 살펴보기 위한 수치해석을 수행하였다. 수치해석 툴로는 오픈소스인 Telemac-2D를 사용하였고, 조석 흐름의 재현을 위한 개방 경계조건을 설정하기 위해서는 동화 조석 모델인 FES2014, NAO99Jb, TPXO9.1 세개의 모델의 데이터로부터 추출된 데이터를 정의하였다. 서해안의 복잡한 지형도 조석에 영향을 미치기 때문에 복잡한 지형의 표현과 그 영향을 고려하기 위해 비정규격자체계를 사용하였다. 수치 해석 결과는 관측자료를 통해 보정 및 검증하였다. 관측자료와 비교하였을 때 수치 해석을 통해 생성된 조석은 관측자료와 잘 부합하였다.

계산 영역에 동일한 값의 마찰계수가 적용된 것과 지역에 따라 다르게 적용한 경우에 서해안에 발생하는 조석에 대하여 평가하였다. 해석 결과 수심과 지형적 특성을 고려하여 마찰 계수를 다르게 적용한 경우 해석 결과가 향상됨을 확인할 수 있었다. 서해안에서의

조석 특성을 파악하기 위하여 개방 조건에 따라 변화하는 조석의 민감도 분석을 수행하였다.

주요어 : 조석 모델, 황해, Telemac, 수치해석, 조석, 비정규격자, 마찰계수

학번 : 2017-21137